PERGAMON

Progress in Biophysics & Molecular Biology 69 (1998) 289–331

Progress in Biophysics & Molecular Biology

Modelling the mechanical properties of cardiac muscle

P.J. Hunter[a,*], A.D. McCulloch[b], H.E.D.J. ter Keurs[c]

[a]*Department of Engineering Science, University of Auckland, Auckland, New Zealand*
[b]*Bioengineering Department, University of California at San Diego, San Diego, CA, USA*
[c]*Department of Medicine and Medical Physiology, University of Calgary, Calgary, Alberta, Canada*

Abstract

A model of passive and active cardiac muscle mechanics is presented, suitable for use in continuum mechanics models of the whole heart. The model is based on an extensive review of experimental data from a variety of preparations (intact trabeculae, skinned fibres and myofibrils) and species (mainly rat and ferret) at temperatures from 20 to 27°C. Experimental tests include isometric tension development, isotonic loading, quick-release/restretch, length step and sinusoidal perturbations. We show that all of these experiments can be interpreted with a four state variable model which includes (i) the passive elasticity of myocardial tissue, (ii) the rapid binding of Ca^{2+} to troponin C and its slower tension-dependent release, (iii) the kinetics of tropomyosin movement and availability of crossbridge binding sites and the length dependence of this process and (iv) the kinetics of crossbridge tension development under perturbations of myofilament length.

1. Background

1.1. Introduction

Finite element models of the electrical and mechanical behaviour of the whole heart are now well established (Hunter and Smaill, 1989; McCulloch, 1995; Hunter et al., 1996a,b). These models take into account the complex three-dimensional ventricular geometry and the anisotropic fibrous-sheet structure of myocardium and thus provide a means of integrating cellular function into the behaviour of the intact heart (see also Vetter and McCulloch, 1997, in this volume). The changes in ion concentrations and membrane ionic currents underlying the cardiac cell action potential are described by the Luo–Rudy equations (Luo and Rudy, 1994;

* Corresponding author.

0079-6107/98/$19.00
PII: S0079-6107(98)00013-3

Zeng et al., 1995) for guinea-pig ventricular cells, or the DiFrancesco–Noble equations (DiFrancesco and Noble, 1985) for Purkinje fibre and atrial cells. There is, however, no corresponding set of published equations encapsulating the mechanical properties of actively contracting cardiac muscle. In this paper we propose a new set of equations describing the full range of mechanical properties of active cardiac muscle.

Since the equations developed here are intended for use in continuum mechanics models of the intact heart, computational efficiency is a major consideration. The equations are not intended to accurately model the biophysical events underlying muscle contraction, but the rate constants can be interpreted in terms of certain biophysical processes. The model we propose here builds on the 'fading memory' model of cross-bridge kinetics first proposed by Bergel and Hunter (1979) and developed further in Hunter (1995).

The model of cardiac muscle mechanics is developed in the following stages: (i) the passive properties of cardiac muscle (since these influence the measurements of active force at low and high sarcomere lengths); (ii) the kinetics of Ca^{2+} binding to troponin C (TnC); (iii) tropomyosin (Tm) kinetics (leading to availability of crossbridge binding sites) and the length dependence of certain parameters in that model and (iv) the crossbridge kinetics associated with myofilament length perturbations.

1.2. Muscle preparations

Published data are available from several species (rat, rabbit, ferret, cat, cow and guinea pig) and different types of preparation: myocardial sheets (typical dimension 500 μm), intact trabeculae (100 μm), skinned myocytes (30 μm) and single myofilaments (1 μm). The mechanical properties of active cardiac muscle are mostly obtained from experiments on small papillary muscles or trabeculae. The muscle cells in these preparations are aligned with the longitudinal axis and, provided muscles with a sufficiently large aspect ratio are used, sarcomere lengths are reasonably constant throughout the muscle cross-section in the central portion of the preparation. Measurement artifacts associated with unavoidable damage to the clamped ends of the preparation can be minimised by measuring the length changes of a central undamaged region (usually with laser diffraction techniques). Intact cardiac muscle can be tetanized by stimulating at a high frequency and using ryanodine or, less desirably, caffeine (which also increases myofibrillar responsiveness to Ca^{2+}) to hold the sarcoplasmic reticular (SR) Ca^{2+} release sites open (Marban et al., 1986; Yue et al., 1986). Controlling free myoplasmic calcium concentration $[Ca^{2+}]_i$ to give a graded response is achieved by controlling the external concentration $[Ca^{2+}]_o$ or with Ca^{2+} channel agonists such as Bay K-8644 (Hess et al., 1984). If intense field stimulation is used it is also common to counter the consequent release of neurotransmitters from the autonomic nerves in myocardium by administering beta-adrenoreceptor blocking agents such as propranolol (Blinks, 1993).

Mechanical experiments are also performed on 'skinned' fibres and single myofibrils. In skinned fibres the cell membrane is dissolved using glycerol or detergents such as Triton X-100 or Lubrol WZ or, for partial permeabilization only, saponin. After chemical skinning the contractile apparatus is left functionally intact and the intracellular calcium concentration is controlled through the use of Ca/EGTA buffers (Gao et al., 1994). The intracellular pH, phosphate concentration and concentration of other ions can also be accurately controlled.

There is evidence that the process of skinning slightly alters the Ca^{2+}-sensitivity of crossbridge binding as we will discuss further below. Single myofibrils are obtained by mincing glycerinated tissue strips, treating with Triton X-100 and then homogenizing in a blender (Linke et al., 1993).

Mitochondria in cardiac muscle cells occupy 40% of the cell volume and it is therefore important to appropriately scale stress measurements from single myofibril preparations to reflect the lower myofilament density in whole myocyte preparations. Some rescaling is also necessary to allow for extracellular material in intact muscle preparations where about 10% of the tissue cross-section is associated with non-contractile material such as capillaries, extracellular collagen and fibroblasts (which outnumber myocytes by two to one).

1.3. Passive elasticity of myocardial tissue

Active tension in intact cardiac muscle is generated within a three-dimensional elastic (or, more accurately, visco-elastic) matrix. For a small range of sarcomere length above slack length (the length of the unloaded, unstimulated muscle) the contribution of the passive elasticity may be neglected, but for sarcomere lengths below 1.85 μm or above 2.2 μm it makes a significant contribution to the total tension. Numerous authors have suggested that extracellular connective tissue, by limiting the lateral expansion of cells, provides an internal load which opposes the actively generated tension in cardiac muscle (e.g. Winegrad, 1980; Huntsman et al., 1983). Externally developed tension in maximally stimulated intact muscle typically falls to zero at a sarcomere length of 1.6–1.7 μm, yet skinned fibres still develop 30% of slack length tension at this length. The fact that there is a clearly defined 'slack length' in intact muscle at 1.85–2.1 μm (depending on species and age) is itself evidence for significant restoring forces.

Recent studies of the microstructure of myocardial tissue (LeGrice et al., 1995) have shown that the myocardium consists of layers of interconnected sheets of tissue separated by 'cleavage planes'. Each sheet is 3 to 4 cells thick (about 100 μm) and loosely coupled together by the perimysial collagen network. The muscle fibres, which lie in the plane of a sheet, are bound together by the endomysial collagen network (predominantly types I and III collagen). Thus adjacent fibres are coupled more strongly in the plane of the sheet than transverse to it. Three micro-structural axes are therefore evident: one along the fibre direction, the *fibre axis*, one orthogonal to the fibre axis but also in the plane of the sheet, the *sheet axis*, and a third, orthogonal to these two, directed across the cleavage planes, the *sheet normal*. The uniaxial stress–strain properties are quite different in the three orthogonal directions, reflecting in part the organization of collagen relative to these three axes (see Fig. 1). In particular, the uniaxial mechanical properties of cardiac muscle in the fibre direction are dominated by large coiled perimysial fibres (MacKenna et al., 1994, 1996).

A fundamental feature of the stress–strain behaviour as the muscle is stretched along an axis is the very steep rise in stress as the limiting elastic strain along each axis is approached (see Fig. 1). For the fibre direction the limiting stretch ratio is about 1.2 (a sarcomere length of about 2.4 μm). Note that muscle length is measured by the muscle fibre extension ratio λ and the actively developed tension in the muscle fibre is denoted by T. The extension ratio λ is the

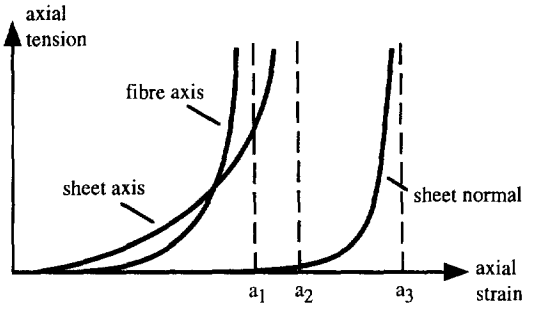

Fig. 1. Uniaxial stress–strain relations along the fibre, sheet and sheet-normal directions. The solid lines show the 'pole-zero' stress–strain relations (see Appendix A) approaching the elastic strain limits a_1, a_2, a_3, respectively.

current sarcomere length divided by the slack length. Here we assume $\lambda = 1$ at a sarcomere length of 2.0 μm.

Intracellular structures provide another source of passive elasticity in muscle (Brady, 1991b). Titin filaments are thought to be responsible for a significant fraction of passive tension for sarcomere lengths below 2.1 μm (Linke et al., 1994; Granzier and Irving, 1995; Granzier et al., 1996, 1997; Helmes et al., 1996). At sarcomere lengths below resting length there is also likely to be an internal elastic load arising from interference between the ends of the thick filament and the Z-lines. The role of internal restoring forces, particularly those arising from titin at sarcomere lengths below 2.1 μm, is discussed by Stuyvers et al. (1997) in this volume.

The passive elastic behaviour of cardiac muscle in tension is modelled in Appendix A, using passive stretch data for intact rat trabeculae from Kentish et al. (1986), and shown as the solid line for $\lambda > 1$ in Fig. 2. The effect on fibre axis force of an elastic load arising from lateral stretching of extracellular collagen is also considered in Appendix A using data from biaxial loading experiments (Smaill and Hunter, 1991). Figure 2 shows the resulting tensile compressive force in this fibre axis direction when sarcomere length is reduced below the resting level ($\lambda < 1$).

The effect of adding the passive fibre axis stress to a linear (maximally activated) active tension relation (discussed below) is shown in Fig. 3. At a sarcomere length of 1.7 μm the actively developed tension exactly balances the internal load and external tension is therefore zero.

1.4. Intracellular calcium

The amount of Ca^{2+} translocating from the junctional sarcoplasmic reticulum (SR) sites is estimated to be 30–50 μM[1] (Robertson et al., 1981). Ca^{2+} binds to many sites within the cell, including Ca–ATPase SR sites (and calsequestrin within the SR), calmodulin, mitochondria, myosin, parvalbumin and troponin C (Johnson et al., 1980; Robertson et al., 1981) and the negatively charged inner surface of the sarcolemma (Soeller and Cannell, 1997). The most important binding sites are troponin C (70 μM), calmodulin (20 μM) and sarcoplasmic

[1] 1 μM = 10^{-6} mol per l of wet tissue.

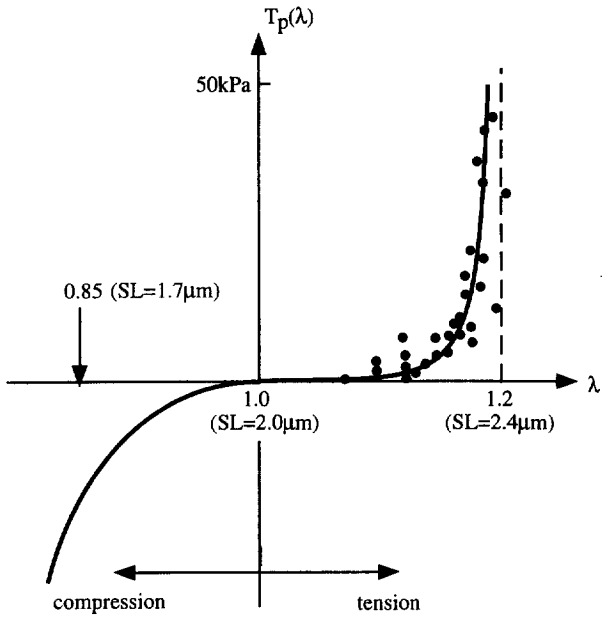

Fig. 2. Passive stress–strain relation in uniaxial tension and compression (see Appendix A). The points (•) are for intact rat trabeculae from Kentish et al. (1986). The dashed line on the right shows the pole position (i.e. stretch limit) in tension at $\lambda_1 = \sqrt{1+2a_1} = 1.2$ (a sarcomere length of about 2.4 μm). The point marked at $\lambda = 0.85$ corresponds to the minimum attainable sarcomere length of 1.7 μm. The solid line for $\lambda > 1$ (in tension) is from Eq. (A.3) with $k_1 = 0.2$ kPa, $a_1 = 0.22$ and $b_1 = 1.0$. The solid line for $\lambda < 1$ (in compression) is from Eq. (A.4) with $k_2 = 0.06$ kPa, $a_2 = 0.41$ and $b_2 = 2.5$.

reticulum (30 μM). Troponin C has three binding sites but two of them (the high affinity Ca^{2+}–Mg^{2+} sites) are saturated at resting levels of Ca^{2+} (0.01 μM) and therefore do not regulate myofilament force development. The third (Ca-specific) TnC binding site, present in

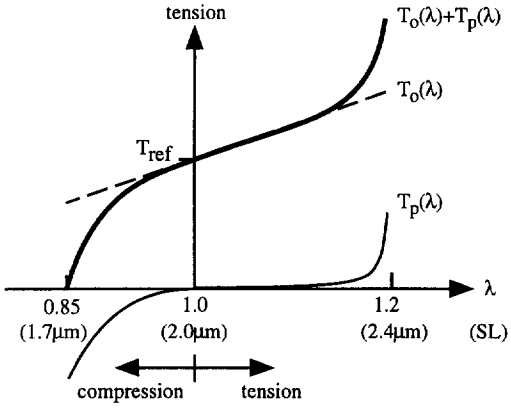

Fig. 3. Tension–length relations for active muscle. The passive tension from Fig. 2 is shown as $T_p(\lambda)$. The total tension (upper solid curve) is the sum of the passive tension and a linear active tension $T_o(\lambda)$ (shown by the dotted line). Sarcomere lengths are indicated at extension ratios of 1.0 (resting length), 1.2 (maximum extension) and 0.85 (minimum extension). The active tension at resting length, T_{ref}, is about 100 kPa.

cardiac myocytes at a concentration of 70 μM, is the regulatory site (Shiner and Solaro, 1984). Binding to TnC is essentially instantaneous and limited only by the speed of diffusion from the junctional SR Ca^{2+}-release sites (a delay of about 0.5 ms). Consequently the Ca^{2+} transient (a measure of cytoplasmic Ca^{2+}) typically rises to a peak of only 1 μM. However, since substantial changes in the time course of decline of the Ca^{2+} transient can occur without affecting force, the fall in $[Ca^{2+}]$ is evidently not the rate limiting step in relaxation of force, which is more likely to be determined by the dissociation of Ca^{2+} from TnC (see later). Mitochondrial Ca^{2+} uptake may be important in sequestering Ca^{2+} during the early part of relaxation (Fry et al., 1989; Wier, 1990).

A single stimulation of an intact muscle held at constant length $\lambda = 1$ (a muscle 'twitch') produces a rapid rise in $[Ca^{2+}]_i$, peaking at 1 μM in about 50 ms, as shown by the points in Fig. 4 from Stuyvers et al. (1997) for rat trabeculae. An external Ca^{2+} concentration of 2.5 mM (or a lower concentration but with paired pulse stimulation) is sufficient to saturate the troponin Ca^{2+} binding sites. For the present purpose we ignore the release and uptake of Ca^{2+} from and to the SR and any diffusional gradients of Ca^{2+} within the myoplasm. A convenient approximate representation of the intracellular Ca^{2+} twitch transient is given by (see solid line in Fig. 4):

$$Ca_i(t) = Ca_o + (Ca_{max} - Ca_o)\frac{t}{\tau_{Ca}} e^{1-t/\tau_{Ca}}. \quad (1)$$

$Ca_i(t)$ here is the time-dependent intracellular concentration of Ca^{2+}, which has a resting level Ca_o and achieves its maximum value Ca_{max} at time $t = \tau_{Ca}$. The solid line in Fig. 4 is from Eq. (1) with $Ca_o = 0.01$ μM, $Ca_{max} = 1$ μM and $\tau_{Ca} = 60$ ms.

Since the release of Ca^{2+} from the junctional SR occurs typically at a concentration of 50 μM, the fact that the twitch reaches only about 1 μM reflects the very large buffering capacity of calmodulin (50 μM) and TnC (70 μM) and, in particular, the very rapid binding of Ca^{2+} to TnC, which we consider in Section 2.

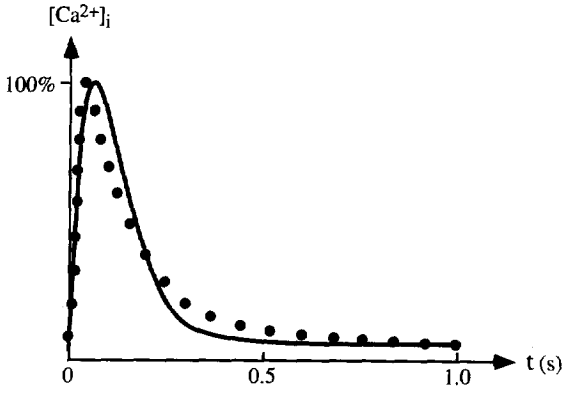

Fig. 4. Calcium transient. Points (•) are from Stuyvers et al. (1997) and solid line is from Eq. (1) with $Ca_0 = 0.01$ μM, $Ca_{max} = 1$ μM and $\tau_{Ca} = 60$ ms. A single exponential model does not quite capture the measured calcium decline.

2. Model development

2.1. TnC–Ca^{2+} binding kinetics

The binding and release of Ca^{2+} from TnC can be studied directly with analogues of TnC which fluoresce in proportion to bound Ca^{2+} (Zot et al., 1986; Zot and Potter, 1987), or by the double isotope technique for chemically skinned fibres (Pan and Solaro, 1987). Binding is very fast and in fact appears to be limited by diffusion gradients from the junctional SR release site to the TnC binding site. The release of Ca^{2+} from the TnC binding site has long been known to be dependent on the mechanical state of the muscle. For example, an isotonic twitch terminates much more quickly than an isometric twitch and if a muscle is subjected to a quick release during a twitch its ability to generate force decays rapidly (Edman, 1975). It is now generally agreed that both of these phenomena are explained by Ca^{2+} being released from the TnC binding site when the myofilament force declines. An increase in TnC–Ca^{2+} affinity associated with the formation of rigor bonds between myosin and actin has been demonstrated for skeletal TnC by Bremel and Weber (1972) and for cardiac TnC by Hofmann and Fuchs (1987a,b). The release of Ca^{2+} from TnC, seen by the rise in intracellular Ca^{2+}, following a reduction in muscle length (isotonic twitches or quick release) was shown by Allen and Kentish (1988) to correlate with a change in tension and not length. This has since been confirmed by other studies (e.g. Janssen and Hunter, 1995). The calcium transient declines more rapidly at longer lengths because the slower release of Ca^{2+} from TnC allows the SR and sarcolemmal Ca^{2+} pumps and Na^+/Ca^{2+} exchanger to lower Ca^{2+} more rapidly (Allen and Kurihara, 1982). Mechanical perturbations have been used by Petersen et al. (1991) to assess the amount of bound calcium during the relaxation phase of a twitch contraction in intact rabbit papillary muscles.

To model these phenomena we propose the following equation for TnC–Ca^{2+} binding kinetics:

$$\frac{dCa_b}{dt} = \rho_0 Ca_i(Ca_{bmax} - Ca_b) - \rho_1\left(1 - \frac{T}{\gamma T_o}\right)Ca_b, \tag{2}$$

where Ca_i is the concentration of free myoplasmic Ca^{2+} and Ca_b is the concentration of Ca^{2+} bound to the Ca-specific binding site on TnC. The maximum value Ca_{bmax} is attained at equilibrium when $T = \gamma T_o$. Attachment is governed by a fixed rate constant ρ_0, estimated to be 100 s^{-1} per μM of available Ca^{2+} (Hilgemann and Noble, 1987). Detachment at zero tension T is governed by the rate constant ρ_1 and as T increases towards a maximum value γT_o, the release rate slows down proportionately.

The equilibrium relationship from Eq. (2),

$$\frac{Ca_b}{Ca_{bmax}} = \frac{Ca_i}{Ca_i + (\rho_1/\rho_0)(1 - T/\gamma T_o)}, \tag{3}$$

is compared in Fig. 5(a) with experimental measurements of bound Ca by Hofmann and Fuchs (1987a,b) using the recorded values of tension from papillary muscles of cow hearts. The ratio of detachment and attachment rates, ρ_1/ρ_0, is found as follows: Hofmann and Fuchs (1987a,b) also recorded levels of bound Ca after treatment by vanadate, which prevents crossbridge binding (by forming a myosin–ADP–Vi complex). At maximum activation (Ca = 10 μM) the tension relative to the maximum value obtained without vanadate treatment is 0.86. Putting

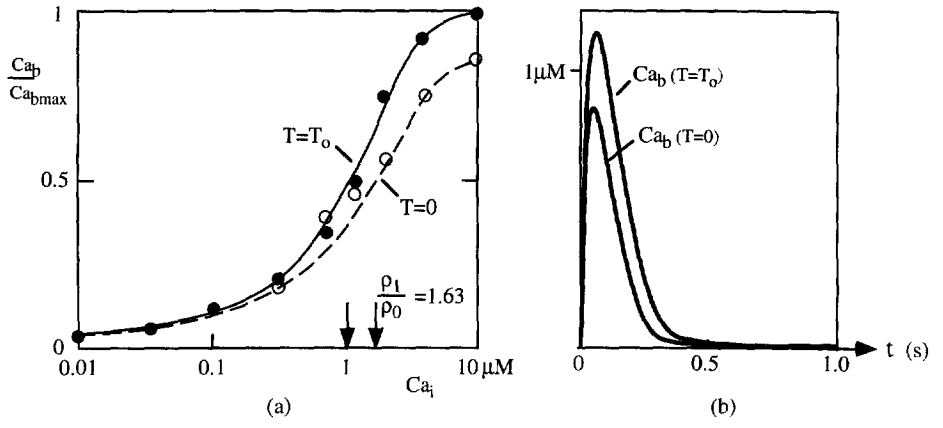

Fig. 5. (a) Relationship between calcium bound to TnC (Ca_b) and intracellular free calcium concentration Ca_i. Points (•) are from Fig. 5 of Hofmann and Fuchs (1987b) and the solid line is Eq. (3) using $T = T_o$, $\gamma = 2.6$ and $\rho_1/\rho_0 = 1.63$ μM. When vanadate is used to prevent crossbridge binding ($T = 0$) the level of bound Ca is reduced (○ points). The broken line is Eq. (3) with the same parameters but $T = 0$. Downward pointing arrows indicate the C_{50} concentrations (see text). (b) Time course of bound calcium using the calcium transient given by Eq. (1). The dependence on crossbridge binding is illustrated by showing the two extremes $T = 0$ and $T = T_o$ (isometric).

$Ca_i = 10$ μM, $T/\gamma T_o = 0$ and $Ca_b/Ca_{bmax} = 0.86$ in Eq. (3) gives $\rho_1/\rho_0 = 1.63$ μM and hence the maximum 'off' rate coefficient $\rho_1 = 163$ s^{-1}. The broken line in Fig. 5(a) shows the TnC–Ca^{2+} binding relationship given by Eq. (3) when crossbridge binding is blocked ($T/\gamma T_o = 0$) and then the Ca level required to give 50% of maximal bound Ca (C_{50}) is $\rho_1/\rho_0 = 1.63$ μM (as indicated by the right downward pointing arrow in Fig. 5(a)). When crossbridge binding is allowed to occur the observed C_{50} is about 1 μM or 0.61 ρ_1/ρ_0 (as indicated by the left downward pointing arrow in Fig. 5(a)). Since the Hofmann and Fuchs measurements were made under steady state conditions, $T = T_o$ and $1 - T/\gamma T_o = 1 - 1/\gamma = 0.61$ gives $\gamma = 2.6$. The isometric binding relationship predicted by Eq. (3) with $\gamma = 2.6$ is shown by the solid line in Fig. 5(a).

The time course of bound Ca in response to the intracellular calcium transient given by Eq. (1) (Fig. 4), is shown in Fig. 5(b) for $T = 0$ and for the isometric case $T = T_o$.

It should be noted that there has been much discussion in the literature recently regarding the influence on crossbridge interaction and Ca^{2+}–TnC binding of increased lateral separation of actin and myosin filaments at short lengths (Wang and Fuchs, 1994, 1995; Fuchs, 1995; McDonald and Moss, 1995). Osmotic compression with 5% Dextran T-500 has been shown to restore crossbridge interaction at short sarcomere lengths, as measured by the resulting inhibition of ATPase activity (Fuchs and Wang, 1996, 1997). Current evidence suggests that the lateral separation of myofilaments directly affects the tension–length relation (see later) and thereby indirectly affects Ca^{2+}–TnC binding via the influence of crossbridge binding on calcium release from TnC. It therefore does not need to be included in Eq. (2).

2.2. Thin filament kinetics

Ca^{2+} binding to TnC initiates a chain of events in the thin filament which results in myosin head binding to actin and the development of force (Holmes, 1995). Tight binding of

TnC–Ca^{2+} to TnI (the inhibitory subunit of troponin) weakens TnI–actin interaction and alters the TnT–Tm complex in such a way that tropomyosin (Tm) moves into the groove of the thin filament, thereby removing a steric obstruction of the actin-crossbridge reaction (Solaro, 1993). Note that shifts in the second actin X-ray diffraction layer line give direct evidence of tropomyosin movement associated with Ca^{2+} binding (Kress et al., 1986).

Skinned fibres are more useful than intact fibres for examining the role of thin filament proteins in the regulation of tension development kinetics because the level of activation by Ca^{2+} can be directly controlled. The following techniques are used:

(1) Rapid release of an isometrically contracting fibre followed by a period of unloaded shortening to reduce the numbers of attached crossbridges and then rapid restretch to its initial length. The remaining crossbridges are thereby detached and tension redevelops from zero at the chosen sarcomere length. The rate constant k_{tr} of tension redevelopment with this techniques varies about 4-fold over the physiological range of Ca^{2+} for cardiac fibres (Wolff et al., 1995). It should be noted here that tension redevelopment following a rapid change in length ('length step' protocol) or length change followed by unloaded shortening and restretch ('ramp/restretch' protocol) may be the result of several distinct physical processes: one is the tension dependent binding of Ca^{2+} to TnC (discussed in Section 2.1), another is the bound-Ca^{2+} dependent movement of Tm and the associated weak to strong transition of bound crossbridges (discussed in this section) and a third is the kinetics of strongly bound crossbridges (discussed in Section 2.3). If length steps are sufficiently small that crossbridges stay attached only the last of these processes is involved. If, however, crossbridges become detached (especially by the ramp/restretch protocol) the first two processes can also be expected to play a part. Whether all of the processes involved in tension redevelopment are Ca^{2+} dependent is controversial and is complicated by the differences between skeletal and cardiac muscle. In fast skeletal muscle there is a 10 to 15-fold increase in the rate constant k_{tr} over the normal operating range of Ca^{2+} (Brenner, 1988; Metzger and Moss, 1990). In slow skeletal muscle, such as rabbit psoas muscle, there is a smaller, 4-fold, increase. In cardiac muscle the evidence is still controversial. The rate of force redevelopment following a rapid length release of intact ferret trabeculae is independent of Ca^{2+} (Hancock et al., 1993) but force redevelopment following rapid release and restretch of skinned rat trabeculae does show Ca^{2+} dependence (Wolff et al., 1995). We suggest that the Wolff et al. (1995) results are explained by thin filament kinetics whereas the Hancock et al. (1993) results are explained by crossbridge kinetics and are therefore discussed later in Section 2.3.

Note that the magnitude of length step in these experiments must be kept small to avoid the influence of shortening deactivation (the displacement of bound calcium from troponin C, see Section 3.4). Vandenboom et al. (1997) report a 17% reduction in force redevelopment rate, which they attribute to shortening deactivation, as the step size applied to single frog skeletal muscle fibres was doubled from 2.5 to 5% of muscle length.

(2) Photorelease of caged ATP in rigor fibres in the presence of Ca^{2+} initiates crossbridge detachment, followed by reattachment and tension redevelopment with rate constant k_{tr} in skeletal muscle (Walker et al., 1992) and cardiac muscle (Barsotti and Ferenczi, 1988; Martin and Barsotti, 1994a,b). In these experiments k_{tr} is less dependent on Ca^{2+} possibly because rigor bridges maintain the thin filament regulatory system in a more fully activated state at all Ca^{2+} levels (Walker and Moss, 1990).

(3) Pulse photolysis of a photosensitive Ca chelator ('caged Ca') to rapidly elevate Ca^{2+} in the vicinity of the myofilaments leads to tension development kinetics very similar to (1) in skeletal muscle (Ashley et al., 1991) and cardiac muscle (Araujo and Walker, 1994, 1996).

2.2.1. Tropomyosin kinetics

To model tropomyosin kinetics we introduce a non-dimensional parameter z ($0 \leq z \leq 1$), representing the proportion of actin sites available for crossbridge binding. Tropomyosin movement resulting from TnC–Ca^{2+} binding controls the availability of these sites and, since tension increases exponentially with a first order rate constant that depends on the level of calcium activation, we propose first order kinetics for z of the form

$$\frac{dz}{dt} = \alpha_0 \left[\left(\frac{Ca_b}{C_{50}} \right)^n (1 - z) - z \right], \tag{4}$$

where α_0 is the rate constant of 'Tm movement' and C_{50} and n are the Hill parameters fitted to the equilibrium relationship between z and Ca_b at a given sarcomere length, i.e. under steady state conditions Eq. (4) gives

$$z_{SS} = \frac{(Ca_b)^n}{(Ca_b)^n + (C_{50})^n}, \tag{5}$$

where C_{50} is the value of Ca_b required to achieve 50% availability ($z_{SS} = 0.5$) and n governs the steepness of the curve. Under the assumption that steady state force is proportional to the number of available actin crossbridge binding sites, z_{SS} is the ratio of the isometric tension T_o to its maximum value T_{omax} obtained at saturating levels of Ca_b. Thus, $z_{SS} = T_o/T_{omax}$.

The exponential change in z following a step change to a new level is obtained from Eq. (4) by substituting

$$z = z_{SS} + Ae^{-k_{tr}t}$$

to give

$$k_{tr} = \alpha_0 \left[1 + \left(\frac{Ca_b}{C_{50}} \right)^n \right]. \tag{6}$$

Figure 6(a) shows the S-shaped equilibrium relationship given by Eq. (5), with $z_{SS} = 0.5$ at $Ca_b = C_{50} = 1$ μM. The rate constant k_{tr} is plotted as a function of Ca_b from Eq. (6) in Fig. 6(b).

Figure 7(a) shows the experimentally measured time course of normalised tension change in response to step changes in Ca^{2+} at various Ca^{2+} levels (Araujo and Walker, 1994). The corresponding rate constant k_{tr} for an exponential fit to these data is shown as a function of z_{SS} ($= T_o/T_{omax}$) in Fig. 7(b). The points are from skinned rat ventricular myocytes and skinned rabbit psaos fibres and the solid line is the predicted dependence of k_{tr} on the normalised isometric tension T_o/T_{omax} as obtained from Eqs. (5) and (6):

$$k_{tr} = \frac{\alpha_0}{1 - z_{SS}}. \tag{7}$$

Note that $k_{tr} = \alpha_0 = 2\ s^{-1}$ at $z_{SS} = 0$.

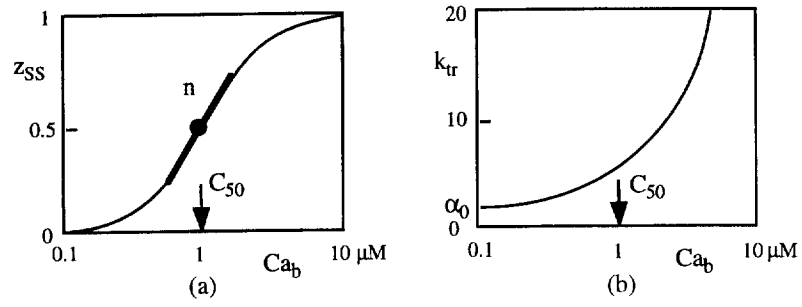

Fig. 6. (a) Equilibrium relationship between actin site availability (z_{SS}) and bound Ca (Ca_b) given by Eq. (5). (b) Rate constant for tension redevelopment k_{tr} given as a function of Ca_b by Eq. (6). The Hill parameters for these plots are $C_{50}=1$ μM and $n = 4.5$ and the rate constant of tropomyosin movement is $\alpha_0=2$ s^{-1} (shown as the limiting value of k_{tr} as $Ca_b \rightarrow 0$ in (b)).

Similar results are obtained from experiments by Wolff et al. (1995) who examined the kinetics of isometric tension development during steady activation in detergent-permeabilised rat ventricular trabeculae. A brief, rapid release and restretch (back to the pre-stretch length) resulted in an exponential recovery of tension whose time constant exhibits a similar 5-fold increase with isometric tension.

2.2.2. *Steady state length dependence*

We next consider the direct effect of myofilament length on tension development under steady state conditions. Length-dependent shifts in Ca^{2+} sensitivity in the physiological range of sarcomere lengths were first reported by Endo (1972) for skinned frog skeletal fibres and by Hibbert and Jewell (1982) for chemically skinned rat ventricular muscle. As mentioned in Section 2.1, the first direct evidence that 'length-dependent' effects on Ca^{2+} binding to cardiac TnC are mediated via crossbridge attachments was provided by Hofmann and Fuchs (1987a,b),

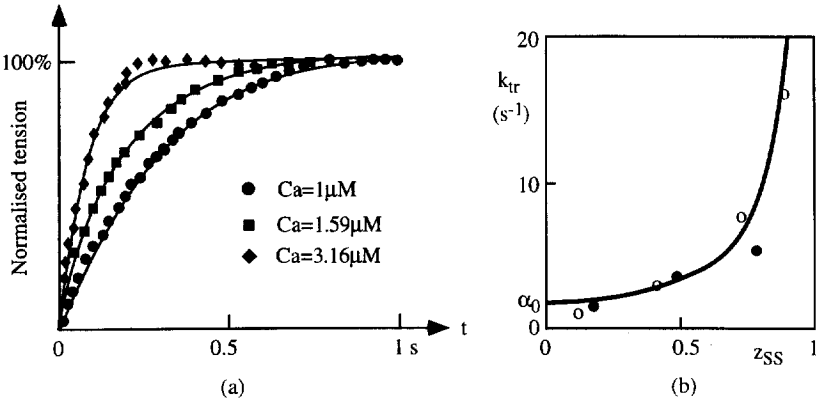

Fig. 7. (a) Time course of normalised cardiac muscle tension development for three Ca^{2+} levels as indicated. (b) Rate constant k_{tr} as a function of z_{SS} for skinned rat ventricular myocytes (•), skinned rabbit psaos fibres (○) and Eq. (7) with $\alpha_0=2$ s^{-1} (solid line). Experimental data is from Araujo and Walker (1994) with 1 mM free Mg^{2+}. (Reducing Mg^{2+} from 1 to 0.1 mM doubles k_{tr} at all levels of Ca^{2+}.)

who showed that when crossbridge attachment is prevented the length dependence of Ca^{2+} binding disappears. However, this is an indirect length dependence since strong crossbridge binding is the key influence.

The direct length dependence of steady state muscle tension at various constant levels of intracellular calcium was first measured by Fabiato and Fabiato (1976, 1978) in skinned cardiac fibres and by ter Keurs et al. (1980b) in intact rat trabeculae. Fig. 8 shows actively developed tension/length data for skinned rat right ventricular muscle from Kentish et al. (1986). At maximum activation the isometric tension–length relation $T_o(\lambda)$ is linear with a slope $dT_o/d\lambda = 145$ kPa, or

$$T_o = T_{ref}(1 + \beta_o(\lambda - 1)), \tag{8}$$

where $T_{ref} = 125$ kPa is the reference tension at $\lambda = 1$ and $\beta_o = 1/T_{ref}\ dT_o/d\lambda = 1.45$. If the increase in tension with length came about solely as a result of changing myofilament overlap, this parameter would be $\beta_o = 1$. Thus, $\beta_o > 1$ reflects myofilament 'cooperativity' (Bremel and Weber, 1972; Butters et al., 1993).

For less than full activation the dependence on Ca under isometric conditions is given by

$$T_o = T_{ref}(1 + \beta_o(\lambda - 1)) \cdot z, \tag{9}$$

where $z = z_{SS}$ is given by Eq. (5) under steady state conditions but otherwise is obtained from the solution of Eq. (4). The experimental measurements from Kentish et al. (1986) shown in

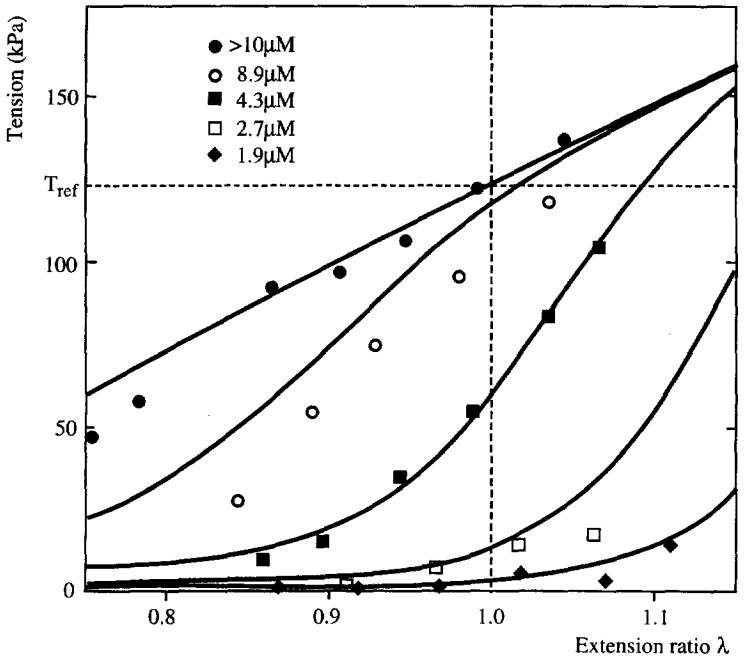

Fig. 8. Isometric tension–length relations for various levels of $[Ca^{2+}]_i$. Points are from skinned rat right ventricular muscle (Fig. 6(B) of Kentish et al., 1986) and solid lines are from Eqs. (9)–(12) with $T_{ref} = 125$ kPa, $n_{ref} = 4.25$, $pC_{50ref} = 5.33$, $\beta_0 = 1.45$, $\beta_1 = 1.95$, $\beta_2 = 0.31$.

Fig. 8 clearly indicate that the linear relationship evident at maximum activation is not preserved at lower levels of bound calcium. The parameters n and C_{50} in Eq. (5) must therefore be length dependent. We have found that giving n and pC_{50} linear length dependence is sufficient to model the full range of $T_o(\lambda, Ca)$. i.e. let

$$z_{SS} = \frac{(Ca)^n}{(Ca)^n + (C_{50})^n} \tag{10}$$

with

$$n = n_{ref}(1 + \beta_1(\lambda - 1)) \tag{11}$$

and

$$pC_{50} = pC_{50ref}(1 + \beta_2(\lambda - 1)) \tag{12}$$

where $C_{50} = 10^{6\text{-}pC_{50}}$ (μM). Choosing $T_{ref} = 125$ kPa, $\beta_0 = 1.45$, $n_{ref} = 4.25$, $\beta_1 = 1.95$, $pC_{50ref} = 5.33$ and $\beta_2 = 0.31$ in Eqs. (9)–(11) to fit the Kentish et al. (1986) data yields the solid lines in Fig. 8.

Note that Eq. (10) absorbs both the Ca_b saturation curve, Eq. (5), and the Ca_i–Ca_b binding relation, Eq. (3). This is illustrated in Fig. 9, where the Ca–TnC binding curve with $T = 0$ (Eq. (3)), shown in Fig. 9(a), together with $Ca_{bmax} = 2.26$ μM and the function $z_{SS}(Ca_b)$ from Eq. (5) with $n = 5.75$, shown in Fig. 9(b), gives the dependence of z_{SS} on Ca_i for $\lambda = 1$ shown by the solid line in Fig. 9(c). This is well approximated by the broken line in Fig. 9(c) (from Eq. (10)) representing the combined saturation behaviour of TnC and Tm, using $n = 4.25$, i.e. the Hill coefficient in the tropomyosin $z_{SS}(Ca_b)$ relation needs to be about 1.5 units higher than the combined $z_{SS}(Ca_i)$ relation and Ca_{bmax} is chosen to match z_{SS} at the C_{50} point for the two Hill relations.

Note that in the model developed here the length dependent Ca^{2+} sensitivity of tension is expressed via Eqs. (10)–(12), where Ca in Eq. (10) is bound calcium Ca_b. This is independent of TnC–Ca^{2+} binding and is justified by experiments with transgenic mice in which cardiac TnC is replaced by fast skeletal TnC (McDonald et al., 1995). For both normal and transgenic

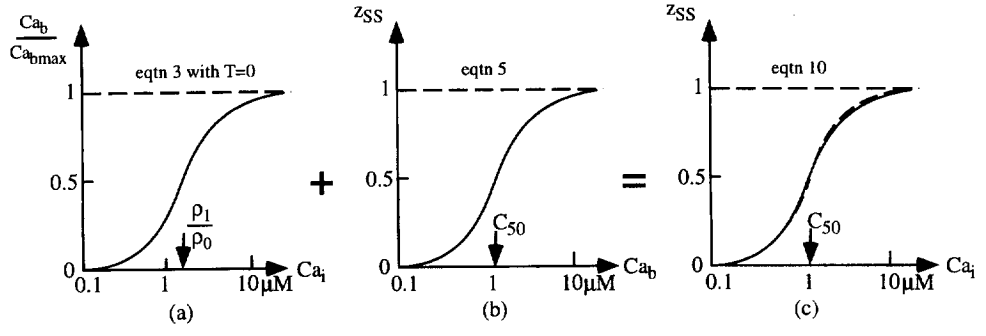

Fig. 9. Hill binding relations for (a) normalised bound calcium Ca_b as a function of intracellular calcium Ca_i (50% saturation at $Ca_i = \rho_1/\rho_0 = 1.63$ μM; see Eq. (3) with $T = 0$); (b) steady state actin site availability z_{SS} as a function of Ca_b (see Eq. (5)) and (c) z_{SS} as a function of Ca_i; see Eq. (10). See text for details.

Table 1

	Refs.	Temp (°C)	SL (μm)	Mg (μM)	Hill coeff.	C_{50} (μM)
Intact rat r.v.	1	20–22	2.2–2.3		4.87 ± 0.35	0.62 ± 0.03
Intact ferret r.v.	2				6.08 ± 0.68	0.50 ± 0.04
Intact rat r.v.	3	20–22	2.1–2.3	5.23 ± 1.18	0.65 ± 0.19	
Skinned rat r.v.	1	20–22		0.72	2.72	2.2
Skinned rat r.v.	1	20–22		0.50	3.75 ± 0.37	0.93 ± 0.1
Skinned rat r.v.	4	22–24	2.15	1.00	4.54 ± 0.74	3.77 ± 0.32

1: Gao et al. (1994) ($n = 10$), 2: Yue et al. (1986) ($n = 7$), 3: Backx et al. (1995) ($n = 9$), 4: Kentish et al. (1986) ($n = 5$).

mice the pC_{50} of the T_o/pCa relationship was shifted 0.12 pCa units in the direction of lower Ca^{2+} as sarcomere length was increased from 1.83 to 2.23 μm indicating no difference in length sensitivity between the two TnC phenotypes. Gulati et al. (1991), on the other hand, do find a reduction in TnC length sensitivity when fast skeletal TnC is substituted for cardiac TnC. A range of values for n and C_{50} is given in Table 1 together with the experimental conditions under which they were obtained.

The steepness of the T_o–Ca relation (i.e. the value for n) is greater for intact fibres than skinned fibres (Gao et al., 1994). Some of the difference is attributable to Mg^{2+} since higher $[Mg^{2+}]_i$ reduces Ca sensitivity (shallower, right-shifted T_o–Ca curve) and the earlier skinned muscle studies used $[Mg^{2+}]_i > 1$ μM whereas intact muscle has $[Mg^{2+}]_i \sim 0.72$ μM (Gao et al., 1994; Murphy et al., 1989). However, as shown in Table 1, even reducing $[Mg^{2+}]_i$ to 0.5 μM in the skinned fibres does not regain the Ca-sensitivity of intact muscles and some other sensitising factors (such as taurine, carnosine-like compounds and possibly MLC kinase, see later) are lost in the skinned preparation (Gao et al., 1994). Note that Backx et al. (1995) found the average measured stress in intact muscles (113 ± 33 kPa) to be statistically identical to that in the same five muscles after skinning (112 ± 33 kPa).

Note that the C_{50} for the skinned rat trabeculae of Kentish et al. (1986) is anomalously high. For subsequent model development and testing we choose $pC_{50ref} = 6.2$ (giving $C_{50ref} = 0.63$ μM). We also choose $n_{ref} = 6.9$ which is 1.5 units higher than the average ($= 5.4$) measured for the combined relation for the intact preparations in Table 1 (see earlier discussion).

An alternative way of presenting $T_o(\lambda, Ca)$ is given in Fig. 10, where T_o is plotted against Ca for various values of λ. As myofilament length increases the Hill relation shifts leftwards and steepens. This behaviour has been reported by many groups (Kentish et al., 1986; Yue et al., 1986; Gulati et al., 1991; Linke et al., 1994).

2.3. Crossbridge kinetics

The model developed so far incorporates Ca^{2+}–TnC binding kinetics (Eq. (2)), tropomyosin kinetics (Eq. (4)) and the steady state length dependence of isometric tension T_o (Eqs. (9)–(12)). In this next stage of model development we analyse crossbridge kinetics by initially assuming a constant level of bound calcium and steady state tropomyosin kinetics, because thin filament kinetics are rather slower than the crossbridge events we will be discussing. The complete

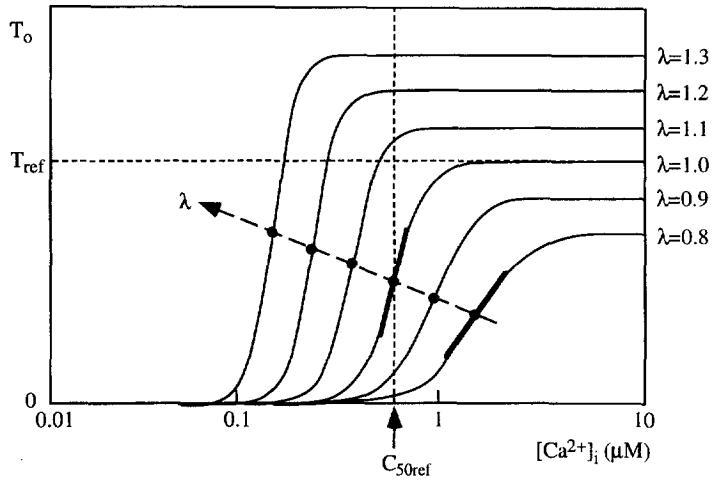

Fig. 10. Steady state isometric tension $T_o(Ca_i)$ given by Eqs. (9)–(12) for six different muscle lengths $\lambda = 0.8$ to 1.3. As length increases the maximum tension, the $[Ca^{2+}]_i$ for 50% maximum tension and the slope (shown for two curves by the thick tangent lines) all increase. The maximum tension for the $\lambda = 1$ (i.e. slack length) curve is T_{ref} and the 50% point for this curve is denoted by C_{50ref}.

model incorporating both thin filament kinetics and crossbridge kinetics will be examined in Section 3.

The most notable feature of the dynamic properties of cardiac (and skeletal) muscle is the fact that very small dynamic length changes are associated with large changes in tension. For example, shortening the muscle by less than 1% of its length in 1 ms produces a 100% drop in tension. Three types of experiment are often used to characterise crossbridge kinetics under a constant level of activation:

- Length step experiments.
- Constant velocity experiments.
- Frequency response experiments.

We use the first and second of these to develop the model and we later compare the model predictions against experimental results for frequency response tests. The tension changes following a rapid length step are shown in Fig. 11(a). Notice (a) the drop in tension concomitant with the length change $\Delta\lambda$ (the lowest tension reached is labelled T_1), (b) the rapid recovery of tension, often with a slight oscillation before (c) a slower recovery to equilibrium. When the experiment is performed from a different initial value of T_0 (e.g. from a different point on the isometric tension–length curve) the entire response is found to scale with T_o. The magnitude of T_1/T_o shows a nonlinear dependence on $\Delta\lambda$, as shown in Fig. 11(b).

2.3.1. Fading memory model

To model these observations of cardiac muscle mechanics we have previously proposed a model (Bergel and Hunter, 1979; Hunter, 1995), called the *fading memory* model, in which a nonlinear function of tension $Q(T, T_0)$ is written as a linear superposition of dynamic length

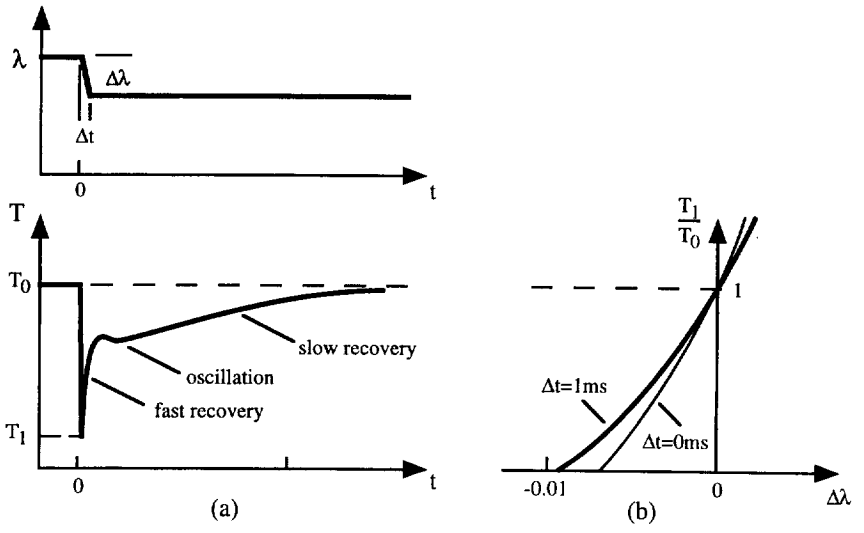

Fig. 11. (a) Tension recovery (lower figure) following a length step of $\Delta\lambda$ in time Δt (upper figure). Notice the different phases of the tension recovery. (b) Tension T_1 reached at the end of the length step, divided by isometric tension T_o, plotted against the magnitude of the length step $\Delta\lambda$. One curve is for a length step of 1 ms duration and the other for an idealised instantaneous step.

changes:

$$Q(T, T_0) = \int_{-\infty}^{t} \phi(t-\tau)\mathring{\lambda}(\tau)\,d\tau, \tag{13}$$

where $\mathring{\lambda} \equiv d\lambda/dt$, $\phi(t)$ is a material response function, and $T_o(\lambda, [Ca^{2+}]_i)$ is the isometric tension–length–Ca^{2+} relation for cardiac muscle given by Eqs. (9)–(12). The justification for this separation of the linear dynamic length changes from the static nonlinear function of tension is the experimental observation that dynamic length changes are small in comparison to the corresponding changes in tension. Under steady state conditions the righthandside of Eq. (13) is zero and the, as yet unspecified, function $Q(T, T_o)$ must be defined such that $Q(T_o, T_o) = 0$. A system defined by Eq. (13) is known in the system identification literature as a 'Wiener cascade model', a linear dynamic system followed by a static nonlinearity.

Two further experimental observations are now used. The first is that all tension measurements on cardiac muscle scale with the isometric tension (this was the justification for using T/T_o in Fig. 11(b)) and therefore $Q(T, T_o) = Q(T/T_o)$. The second is that the current tension is influenced more by recent length changes than earlier length changes, the 'fading memory' assumption. This latter assumption allows the material response function to be written as a sum of exponentials:

$$\phi(t) = \sum_{i=1}^{N} A_i e^{-\alpha_i t}, \tag{14}$$

where α_i and A_i, $i = 1, \ldots, N$, are the exponential rate constants and associated weighting coefficients, respectively.

In fact the tension recovery curves in Fig. 11(a) show evidence of three distinct physical processes: the initial fast recovery with a slight oscillation is indicative of a second order process (e.g. myosin head rotation in the model by Huxley and Simmons, 1971) and the subsequent slow recovery phase is evidence of a first order process (the crossbridge detachment–attachment cycle in the Huxley, 1957, model with the rate limiting step probably being detachment). We therefore limit the number of rate constants N in Eq. (14) to 3 and Eq. (13) becomes

$$Q(T/T_o) = \sum_{i=1}^{3} A_i \int_{-\infty}^{t} e^{-\alpha_i(t-\tau)} \dot{\lambda}(\tau)\, d\tau, \tag{15}$$

where we let α_1 be the rate constant associated with the first order slow tension recovery, and α_2 and α_3 be the rate constants for the second order fast recovery process in Fig. 11(a).

2.3.2. Constant velocity experiments

A parameterised form of the nonlinear function $Q(T/T_o)$ can be determined from constant velocity experiments. In these experiments the muscle is served to shorten at a constant rate, or shortens at a constant rate (following an initial transient) in response to a reduction in tension to a constant value less than T_o. The plot of tension versus velocity is called a *force–velocity curve*. These curves are typically hyperbolic and are accurately described for tetanised (maximally activated) muscle by the equation first proposed by Hill (1938):

$$\frac{-V}{aV_o} = \frac{\dot{\lambda}}{aV_o} = \frac{T/T_o - 1}{T/T_o + a}, \tag{16}$$

where V_o is the maximum velocity (achieved when $T = 0$) and a is a parameter which controls the curvature of the force–velocity relation (the parameter 'a' here is chosen to be non-dimensional, the 'a' in Hill's original equation is equivalent here to aT_o). As with force recovery following a length step, the force–velocity curves scale with isometric tension T_o.

The unloaded shortening velocity V_o has had a special significance for muscle physiologists because it appeared to be independent of length and level of activation, at least for lengths greater than resting length ($\lambda > 1$). For $\lambda < 1$ the passive muscle structures are in compression and the 'unloaded' shortening is then shortening against an internal load (see Section 3.1).

Ignoring the two rate constants α_2 and α_3 associated with the initial transient following the tension step (since this has decayed by the time the force–velocity measurements are made) and putting $\dot{\lambda} = -V$ (the constant velocity of shortening), Eq. (15) reduces to $Q(T/T_o) = -A_1/\alpha_1 V$. An exact match to Hill's classic force–velocity relation (Hill, 1938) is then obtained by choosing $Q(T/T_o) = (T/T_o - 1)/(T/T_o + a)$ and $V_o = \alpha_1/aA_1$, giving

$$\dot{\lambda} = -V = \frac{\alpha_1}{A_1} \frac{T/T_o - 1}{T/T_o + a}. \tag{17}$$

Experimental results from cardiac muscle (de Tombe and ter Keurs, 1990, 1991b, 1992) give a relative velocity (V/V_o) of about 25% at a relative tension (T/T_o) of 50%. Putting $T/T_o = \frac{1}{2}$ in Eq. (17) gives $V/V_o = \frac{1}{2}a/(\frac{1}{2} + a)$ and hence $V/V_o = 0.25$ gives $a = 0.5$.

The maximum (unloaded) shortening velocity found by de Tombe and ter Keurs (1990) for rat trabeculae at 24°C is 11.3 μm·s^{-1} per 1.9 μm sarcomere, or $V_o = 6$ s^{-1} and hence $\alpha_1/A_1 = aV_o = 3$ s^{-1}. They also comment that the temperature dependence of V_o has a Q_{10} of 4.6 (i.e. raising the temperature by 10°C increases V_o by a factor of 4.6) which is consistent with the reported temperature dependence of rat actin-activated myosin ATPase (Barany, 1967).

The fading memory model of crossbridge mechanics is now given by

$$\frac{T/T_o - 1}{T/T_o + a} = \sum_{i=1}^{3} A_i \int_{-\infty}^{t} e^{-\alpha_i(t-\tau)} \mathring{\lambda}(\tau)\, d\tau. \tag{18}$$

It is convenient to express Eq. (18) in the form

$$T = T_o \cdot \frac{1 + aQ}{1 - Q}, \quad \text{where } Q = \sum_{i=1}^{3} A_i \int_{-\infty}^{t} e^{-\alpha_i(t-\tau)} \mathring{\lambda}(\tau)\, d\tau. \tag{19}$$

i.e. the observed tension T is the isometric tension T_o scaled by a nonlinear function of the hereditary integral of length changes.

2.3.3. Length step experiments

The response to an instantaneous length step is found by putting $\lambda(t) = \Delta\lambda \cdot H(t)$ (the Heaviside step function) or $\mathring{\lambda} = \Delta\lambda \cdot \delta(t)$ (the Dirac delta function), in which case Eq. (18) becomes

$$\frac{T/T_o - 1}{T/T_o + a} = \Delta\lambda \cdot \sum_{i=1}^{3} A_i e^{-\alpha_i t}. \tag{20}$$

The tension reached immediately after the step is found by putting $T = T_1$ and $t = 0$ in Eq. (20) to give

$$\frac{T_1/T_o - 1}{T_1/T_o + a} = \Delta\lambda \cdot \sum_{i=1}^{3} A_i. \tag{21}$$

The length step experiments required to evaluate the rate constants from Eq. (20) have been performed for intact tetanised ferret cardiac muscle at 27°C by Hancock et al. (1993). Figure 12 shows the tension response following a 2% length step accomplished in 2 ms (which is just sufficient to drop the immediate post-step tension to zero). The solid line in Fig. 12 is from the single rate constant version of Eq. (20) with $a = 0.5$, $\alpha_1 = 75$ s^{-1} and $A_1 = 50$ (all other crossbridge constants set to zero) and a slope of $(1/T_o)(dT_o/d\lambda) = 17$ in the isometric tension–length relation obtained from the 4.5 mM data in Fig. 2 of Hancock et al. (1993).

Note that the speed of unloaded shortening V_o predicted by the model with these parameters is $V_o = \alpha_1/aA_1 = 3$ s^{-1}, which is somewhat lower than the 6 s^{-1} (see earlier) found by de Tombe and ter Keurs (1990) for rat trabeculae at 24°C. The rate constant $\alpha_1 = 75$ s^{-1} evaluated here for ferret cardiac muscle at 27°C becomes $\alpha_1 = 33$ s^{-1} at 22°C if we assume a Q_{10} of 4.6 for myosin–ATPase (Barany, 1967).

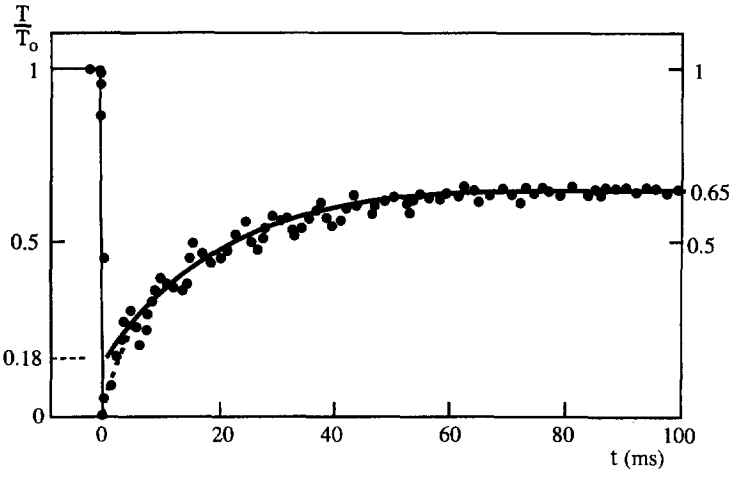

Fig. 12. Tension response to rapid length step. Points (•) are for ferret cardiac muscle at 27°C (Hancock et al., 1993). Solid line is from Eq. (20) with one rate constant and parameters $a = 0.5$, $\alpha_1 = 75\ s^{-1}$ and $A_1 = 50$. The broken line is from Eq. (20) with all three rate constants ($\alpha_2 = \alpha_3 = 2850\ s^{-1}$; $A_2 = A_3 = 175$). The horizontal dotted line at $T/T_o = 0.18$ marks the immediate post-step tension for the single rate constant relation, which is useful for determining the parameter A_1 (see text).

The single time constant model clearly fails to capture the very early tension recovery. The broken line in Fig. 12 shows the result of adding in the other two faster rate constants (see below). We next consider the evaluation of these two rate constants (α_2 and α_3) and their associated scaling constants (A_2 and A_3).

The instantaneous length change $\Delta\lambda_0$ required to drop the tension to zero immediately after the step is found from Eq. (21) by putting $T_1 = 0$:

$$-\Delta\lambda_0 = 1/a\sum_{i=1}^{3} A_i. \tag{22}$$

In practice the inertia of the muscle and testing equipment mean that an 'instantaneous' length step on cardiac muscle actually requires 1 ms or more to complete. We therefore examine the consequences of a finite duration length step and show that Eq. (22) is obtained as the theoretical limit for zero step duration. Note that putting $a = 0.5$ and $-\Delta\lambda_0 = 0.005$ in Eq. (22) (a 0.5% length change to abolish tension) gives $\Sigma_{i=1}^{3} A_i = 400$ which provides one constraint on the values of A_2 and A_3.

2.4. Finite duration length steps

It is difficult to perform length steps fast enough on cardiac muscle to reveal the two fast rate constants. Hancock et al. (1993) achieve 1 ms steps with ferret cardiac muscle compared with steps of 0.2 ms duration by Ford et al. (1977) on single fibre frog skeletal muscle. In this section we show that the data obtained by Hancock et al. (1993) from multiple steps can in fact recover the fast rate constant parameters (α_2, A_2, α_3, A_3) without the need for the much faster steps possible with single skeletal fibres.

The response to a rapid but finite duration length change is found by putting

$$\dot{\lambda} = \begin{cases} 0 & t<0 \\ \dfrac{\Delta\lambda}{\Delta t} & 0<t<\Delta t \\ 0 & t > \Delta t \end{cases}$$

in Eq. (17) (see Fig. 11(a), top) and integrating to give

$$\frac{T/T_o - 1}{T/T_o + a} = \frac{\Delta\lambda}{\Delta t} \cdot \sum_{i=1}^{3} \frac{A_i}{\alpha_i} e^{-\alpha_i t}(e^{\alpha_i \Delta t} - 1). \tag{23}$$

The tension T_1 immediately after the step is found from Eq. (23) by putting $t = \Delta t$ and $T = T_1$:

$$\frac{T_1/T_o - 1}{T_1/T_o + a} = \frac{\Delta\lambda}{\Delta t} \cdot \sum_{i=1}^{3} \frac{A_i}{\alpha_i}(1 - e^{-\alpha_i \Delta t}). \tag{24}$$

Equation (24) gives the plot of T_1/T_o against $\Delta\lambda$ shown in Fig. 11(b). For a step of duration Δt the magnitude of step change required to drop the tension T_1 to zero, from Eq. (24), is

$$-\Delta\lambda = \frac{\Delta t}{a} \sum_{i=1}^{3} \frac{A_i}{\alpha_i} \cdot (1 - e^{-\alpha_i \Delta t}) \tag{25}$$

Figure 13 shows the relationship between $-\Delta\lambda$ and Δt for the previously fitted parameters. Also shown are experimental data for cardiac muscle at 27°C (Hancock et al., 1993) and single fibre frog skeletal muscle at 0°C (Ford et al., 1977). Note the consistency with the model for both ferret cardiac muscle at 27°C and frog skeletal muscle at 0°C. Taking the limit of Eq. (25)

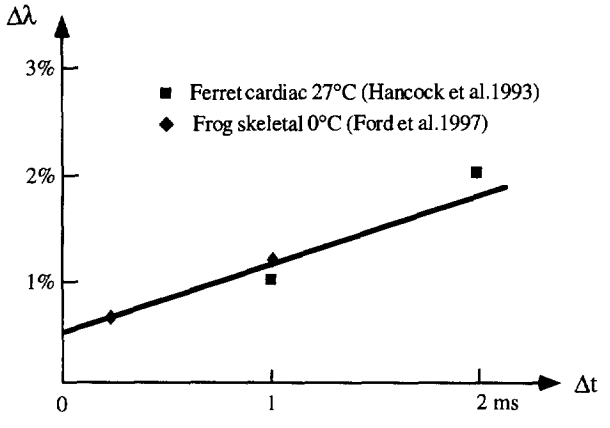

Fig. 13. Magnitude of rapid length step required to drop tension to zero versus duration of step. Points (■) are from Hancock et al. (1993) for ferret cardiac muscle at 27°C and (◆) Ford et al. (1977) for frog skeletal muscle at 0°C. Solid line is Eq. (20) with parameters $a = 0.5$, $\alpha_1 = 33\ s^{-1}$, $\alpha_2 = \alpha_3 = 2850\ s^{-1}$ and $A_1 = 50$, $A_2 = A_3 = 175$.

as $\Delta t \rightarrow 0$ recovers the instantaneous relationship, Eq. (22), derived earlier. The slope of the curve, found by differentiating Eq. (25) with respect to Δt, is nearly constant for $t < 2$ ms and is given at $t = 0$ by

$$s_0 = \frac{d}{d\Delta t}(-\Delta t)|_{\Delta t=0} = \sum_{i=1}^{3} A_i\alpha_i / 2a\left(\sum_{i=1}^{3} A_i\right)^2 \tag{26}$$

or using $a\Sigma_{i=1}^{3} A_i = (-\Delta\lambda_0)^{-1}$ from Eq. (22),

$$\sum_{i=1}^{3} A_i\alpha_i = \frac{2s_0}{a}(-\Delta\lambda_0)^{-2}. \tag{27}$$

Using $a = 0.5$, obtained previously, $-\Delta\lambda_0 = 0.005$ and $s_0 = 6.25$ s^{-1} from Fig. 13, Eq. (27) gives $\Sigma_i^3 A_i\alpha_i = 10^6$ s^{-1}. The single rate constant fit to the Hancock et al. (1993) data gave $\alpha_1 = 75$ s^{-1} and $A_1 = 50$. Since there are insufficient data to distinguish the two rate constants α_2 and α_3, we set $\alpha_2 = \alpha_3$ and $A_2 = A_3$. Then $\Sigma_{i=1}^{3} A_i\alpha_i = 10^6$ s^{-1} from Eq. (27) together with $\Sigma_{i=1}^{3} A_i = 400$ from Eq. (22) gives $A_2 = A_3 = 175$ and $\alpha_2 = \alpha_3 = 2850$ s^{-1}. Note that this compares with values of $\alpha_2 = 1000$ s^{-1} and $\alpha_3 = 5000$ s^{-1} obtained by Bergel and Hunter (1979) for single fibre frog skeletal muscle from data by Ford et al. (1977). It is not clear at this stage whether these two rate constants (determined here from data obtained at 27°C) need to be reduced for 22°C, it would appear from the data shown in Fig. 13 that they are remarkably insensitive to temperature or species.

Following a finite duration length step, the immediate post-step tension T_1 predicted by the model, when only one rate constant is included, is found from Eq. (24). Putting $-\Delta\lambda = 0.02$, $\Delta t = 0.002$ s, $A_1 = 50$, $\alpha_1 = 75$ s^{-1} and $A_2 = A_3 = 0$, Eq. (24) gives $T_1/T_o = 0.28$, where T_o here is 0.65 of the initial isometric tension (used as the normalisation factor for tension in Fig. 12). Therefore $T_1/T_o = 0.28 \times 0.65 = 0.182$ is the fraction relative to the initial isometric tension. This is shown by the dotted line on the left in Fig. 12.

This completes the development of the model. An important feature of the model of crossbridge kinetics proposed here is that all constants (a, α_i, A_i) are independent of both length (λ) and calcium (Ca_i or Ca_b); the influence of λ and Ca_b occurs solely within the model of thin filament kinetics. This is justified for cardiac muscle by the experimental observations of Hancock et al. (1993, 1996) which show the rate constant of tension recovery from a small length step to be independent of both λ and Ca_i.

2.5. Model summary

The complete 'HMT' model is summarised here together with the set of fitted parameters for (primarily rat ventricular) cardiac muscle at 22°C.

Passive elasticity:

Tension: Eq. (A.3), where $k_1 = 0.2$ kPa; $a_1 = 0.22$; $b_1 = 1.0$.

Compression: Eq. (A.4), where $k_2 = 0.06$ kPa; $a_2 = 0.41$; $b_2 = 2.5$.

Calcium transient:

Eq. (1), where $\tau_{Ca} = 0.06$ s; $Ca_o = 0.01$ μM; $Ca_{max} = 1$ μM.

TnC–Ca binding:
Eq. (2), where $\rho_0 = 100\ s^{-1}\ \mu M^{-1}$; $\rho_1 = 163\ s^{-1}$; $\gamma = 2.6$; $Ca_{bmax} = 2.26\ \mu M$.
Thin filament kinetics:
Eqs. (4), (9), (11) and (12), where $T_{ref} = 100$ kPa; $n_{ref} = 6.9$; $pC_{50ref} = 6.2$ and $\alpha_0 = 2\ s^{-1}$; $\beta_0 = 1.45$; $\beta_1 = 1.95$; $\beta_2 = 0.31$.
Crossbridge kinetics:
Eq. (19), where $a = 0.5$; $A_1 = 50$; $\alpha_1 = 33\ s^{-1}$ and $A_2 = A_3 = 175$; $\alpha_2 = \alpha_3 = 2850\ s^{-1}$.

If the free calcium concentration Ca_i and the muscle fibre extension ratio λ are regarded as inputs to the system, these equations constitute a set of four fundamental equations in the four state variables Ca_b, z, T_o and T which may be expressed as

$$Ca_b = f_1(Ca_i, Ca_b, T, T_o) \quad \text{(equation 2)}$$

$$z = f_2(z, \lambda, Ca_b) \quad \text{(equation 4)}$$

$$T_o = f_3(\lambda, z) \quad \text{(equations 9–12)}$$

$$T = f_4(T_o, \lambda, t) \quad \text{(equation 19)}$$

The first two of these are first order ordinary differential equations, the third is an algebraic relation and the last is an hereditary integral.

3. Model predictions

The equations summarised in Section 2.4 have been developed to model a wide range of cardiac muscle mechanical behaviour primarily involving steady state or length step responses. We now examine and test the model in a wider variety of experiments.

3.1. More general tension–velocity relations

A unique relationship between shortening velocity and tension in a tension-step experiment can only exist when the isometric tension does not vary with length and then only when the initial velocity transients have decayed. To find the relationship between velocity, tension and length in a tension-step experiment conducted on the ascending limb of the isometric tension–length curve, consider the single rate constant version of Eq. (18) (applicable once the transient velocity fluctuations have decayed):

$$\frac{T/T_o - 1}{T/T_o + a} = A_1 \int_{-\infty}^{t} e^{-\alpha_1 (t-\tau)} \dot{\lambda}(\tau)\, d\tau. \tag{28}$$

Differentiating Eq. (28) with respect to time, with T constant, gives

$$-\frac{T}{T_o^2} \frac{1+a}{(T/T_o + a)^2} \cdot \frac{dT_o}{d\lambda} \cdot \dot{\lambda} = -\alpha_1 \frac{T/T_o - 1}{T/T_o + a} + A_1 \dot{\lambda}$$

or

$$\mathring{\lambda} = \alpha_1 \frac{T/T_o - 1}{T/T_o + a} \Bigg/ \left\{ A_1 + \frac{1+a}{(T/T_o + a)^2} \cdot \frac{T}{T_o^2} \cdot \frac{dT_o}{d\lambda} \right\}. \tag{29}$$

When $dT_o/d\lambda = 0$, Eq. (29) reduces to Eq. (17), which is plotted in Fig. 14(a).

The maximum shortening velocity V_o is achieved at zero load ($T = 0$) and, from Eq. (29),

$$V_o = -\mathring{\lambda}|_{T=0} = \frac{\alpha_1}{aA_1} \tag{30}$$

is seen to be independent of activation level, muscle length (for $\lambda > 1$ only, see below) and the slope of the isometric tension–length curve. With the parameters obtained earlier for ferret cardiac muscle at 27°C, $a = 0.5$, $\alpha_1 = 75\ s^{-1}$ and $A_1 = 50$, the maximum shortening velocity from Eq. (30) is $V_o = 3\ s^{-1}$.

At 50% load ($T/T_o = 0.5$) and $dT_o/d\lambda = 0$ Eq. (29) gives $-\mathring{\lambda} = 0.75\ s^{-1}$ (i.e. $T = \frac{1}{2}T_o$ gives $V = \frac{1}{4}V_o$). Under maximum activation the slope of the isometric tension curve at $\lambda = 1$ is $(1/T_o)(dT_o/d\lambda) = \beta_o = 1.45$ but this only reduces the shortening velocity by 4% because the coefficient A_1 is relatively large.

At 50% of maximum activation (e.g. $[Ca^{2+}]_i = 5\ \mu M$ in Fig. 8) the slope $(1/T_o)(dT_o/d\lambda)$ is considerably larger and the shortening velocity at 50% load is reduced by about 15%.

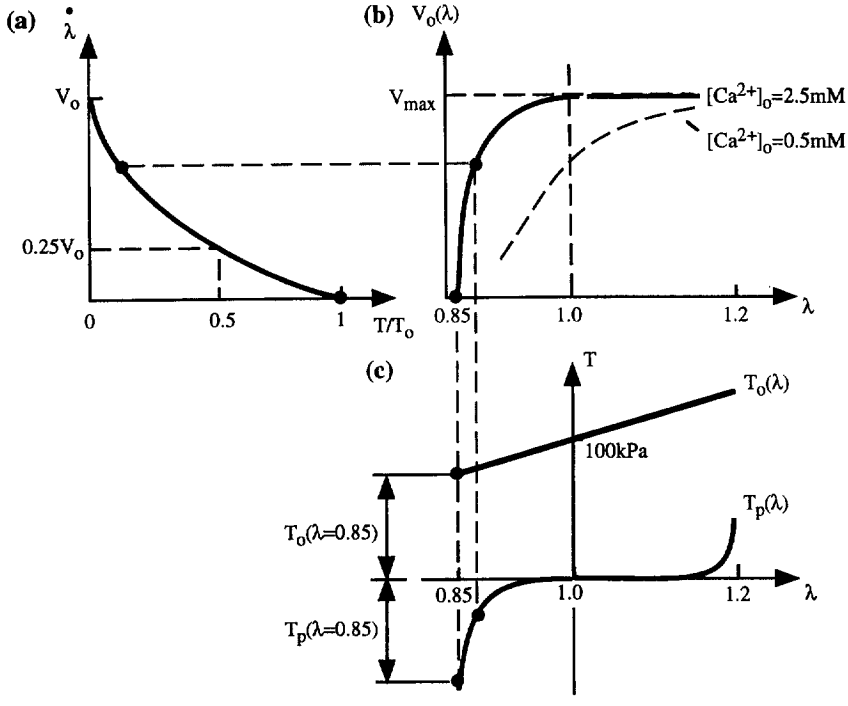

Fig. 14. (a) Shortening velocity at resting length as a function of relative tension. V_o is the velocity when shortening against zero external load. (b) V_o as a function of λ. The decline of V_o for $\lambda < 1$ is a result of the increasing internal compressive load as shown in (c). See text for details.

Note also that the reduction of maximum velocity peaks when the slope of the isometric tension–length relation is maximum at $\lambda = 1$ would then be predicted to diminish. For $\lambda > 1$ these predictions are consistent with the experimental observations by de Tombe and ter Keurs (1990) shown in Fig. 14(b). At very low $[Ca^{2+}]_i$ and $\lambda < 1$ an additional viscous load arising from the titin filaments may further reduce the shortening velocity (see Stuyvers et al., 1997).

The prediction that maximum (unloaded) shortening velocity is independent of activation level and muscle length only holds for $\lambda > 1$ when there is negligible internal load arising from the extracellular matrix or titin filaments. Figure 14 illustrates the effect on shortening velocity of a compressive load when $\lambda < 1$. As the compressive load increases (see Fig. 14c) the muscle moves down its velocity–tension relation (Fig. 14a) and thereby produces the roll-off in velocity with length seen in Fig. 14(b). When the muscle shortens to the point ($\lambda = 0.85$) where the passive compressive stress T_p equals the actively developed stress T_o, V_o is zero, in agreement with the experimental observations of de Tombe and ter Keurs (1990).

3.2. High frequency dynamics

The dynamic stiffness of muscle can be measured by imposing a small sinusoidal length perturbation while it is otherwise isometric or shortening at constant velocity (i.e. against a constant load). Dividing the recorded sinusoidal tension changes by the applied length changes gives a dynamic stiffness. The stiffness predicted by the model at $\lambda = 1$ (see Appendix B, Eq. (B.23)) is the following complex function of perturbation frequency ω and myoplasmic calcium concentration Ca_i:

$$\mathbf{E} = T_o\beta_o + \frac{n_{ref}T_oA\alpha_0}{\alpha_0/(1-z)+i\omega} + T_o\left[1 + \frac{n_{ref}\alpha_0}{\alpha_0/(1-z)+i\omega}\cdot\frac{\rho_1/\gamma}{\rho_0 Ca_i + \rho_1(1-1/\gamma)+i\omega}\right] \times (1+a)\sum_{k=1}^{3} A_k\frac{i\omega}{\alpha_k + i\omega}, \tag{31}$$

where $i=\sqrt{-1}$, $T_o = zT_{ref}$,

$$Ca_b = \frac{Ca_{bmax}Ca_i}{Ca_i + (\rho_1/\rho_0)(1-1/\gamma)}, \qquad z = \frac{(Ca_b)^{n_{ref}}}{(Ca_b)^{n_{ref}} + (C_{50ref})^{n_{ref}}}$$

and

$$A = \beta_1 \ln\frac{Ca_b}{C_{50ref}} + \beta_2 \ln 10 \cdot pC_{50ref}. \tag{32}$$

Note the use of 'k' rather than 'i' as the rate constant index in Eq. (31) to avoid confusion with the complex number i. Also note that T_o, z and Ca_b here are the mean values about which the sinusoidal perturbations occur.

The three components on the righthandside of Eq. (31) are, respectively,

$$\mathbf{E}_1 = zT_{ref}\beta_o \tag{33}$$

is the static stiffness arising from the non-zero slope β_o of the isometric tension–length relation. As might be expected this is directly proportional to the thin filament activation z (i.e. the proportion of actin sites available for crossbridge binding).

$$\mathbf{E}_2 = zT_{\text{ref}} \cdot \frac{n_{\text{ref}} A \alpha_0}{\alpha_0/(1-z) + i\omega} \tag{34}$$

is the stiffness associated with length dependence in the thin filament kinetic equations (e.g. if β_1 and β_2 are zero this stiffness is zero, since $A = 0$ from Eq. (32)). Note that this has a more complex dependence on z and acts as a low pass filter with a break frequency at $\omega = \alpha_0/(1-z)$.

$$\mathbf{E}_3 = zT_{\text{ref}} \cdot \left[1 + \frac{n_{\text{ref}}\alpha_0}{\alpha_0/(1-z) + i\omega} \cdot \frac{\rho_1/\gamma}{\rho_0 \text{Ca}_i + \rho_1(1 - 1/\gamma) + i\omega}\right](1+a)\sum_{k=1}^{3} A_k \frac{i\omega}{\alpha_k + i\omega} \tag{35}$$

is the stiffness associated with crossbridge kinetics combined with the influence of TnC–Ca^{2+} binding and thin filament kinetics. Note that this term has no effect at $\omega = 0$ but becomes dominant at high frequencies. The crossbridge stiffness acts as a high-pass filter with break frequencies at $\omega = \alpha_1$, α_2 and α_3. At lower frequencies the crossbridge stiffness is modulated by the low-pass filtering characteristics of TnC–Ca^{2+} binding and thin filament kinetics.

The dynamic stiffness given by Eq. (31) is shown in Fig. 15 as a Bode plot (magnitude $|\mathbf{E}|$ and phase Φ plotted against frequency ω) for two values of Ca_i. The previous parameter set, used for this plot, gives stiffness magnitude increasing monotonically with ω. A small dip has been reported in some studies (Rossmanith et al., 1986). The model can reproduce such a dip at low frequencies (when A in Eq. (32) is negative at low Ca_b) but only with a larger value of β_1 than the one obtained earlier.

Note that the low frequency break point at $\omega = \alpha_0/(1-z)$ in Fig. 15 increases as z increases. From Eq. (31) the steady state stiffness ($\omega = 0$) is

$$E|_{\omega=0} = T_{\text{ref}}[z\beta_o + n_{\text{ref}} A z(1-z)]. \tag{36}$$

which falls to zero at $z = 0$ and $z = 1$ and achieves its maximum at $z = \frac{1}{2} + \beta_0/2n_{\text{ref}}A$.

At perturbation frequencies above about $\omega = \alpha_1 = 33\ s^{-1}$, the first two stiffness terms $\mathbf{E}_1$ and $\mathbf{E}_2$ are negligible and the response is dominated by the crossbridge stiffness $\mathbf{E}_3$. The limiting stiffness at high frequency is

$$E|_{\omega=\infty} = zT_{\text{ref}}\left[\beta_o + (1+a)\sum_{k=1}^{3}\frac{A_k}{\alpha_k}\right], \tag{37}$$

and, since the first term on the right in Eq. (37) is small compared with the second term, high frequency stiffness is proportional to the number of available crossbridge binding sites z (or, equivalently, isometric tension T_o).

3.3. High frequency stiffness during isotonic shortening

An experiment that has been performed on single skeletal muscle fibres (but not yet on cardiac muscle) is to impose a small high frequency oscillation during isotonic shortening

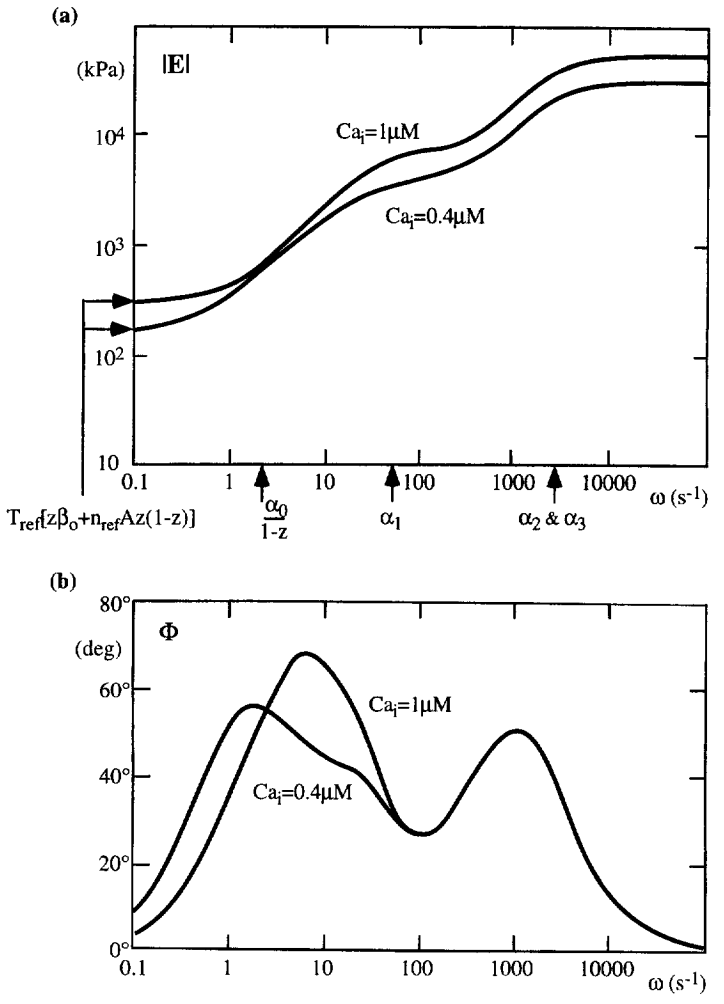

Fig. 15. Muscle stiffness predicted by the model. (a) Modulus versus frequency for two different levels of calcium activation ($Ca_i = 0.4$ μM, 1 μM). The three upwardly directed arrows show the locations of the four breakpoint frequencies ($\alpha_0/(1-z)$, α_1, α_2 and α_3) corresponding to the rate constants of thin filament and crossbridge kinetics. (b) Phase angle versus frequency for the same two activation levels. The influence of the fast crossbridge rate constants α_2 and α_3 is seen in the second peak.

against a load T and to plot this stiffness $E(T, T_o, \omega)$ relative to the isometric stiffness $E(T_o, T_o, \omega)$ as a function of relative tension T/T_o. This relationship, derived in Appendix B (Eq. (B.5)) for the plateau of the isometric tension–length relation, is:

$$\frac{E(T, T_o, \omega)}{E(T_o, T_o, \omega)} = \left(\frac{T/T_o + a}{1 + a}\right)^2. \tag{38}$$

Equation (38) is plotted in Fig. 16 together with experimental data for single frog skeletal fibres at 0°C from Julian and Sollins (1975). A notable feature of the relationship is the

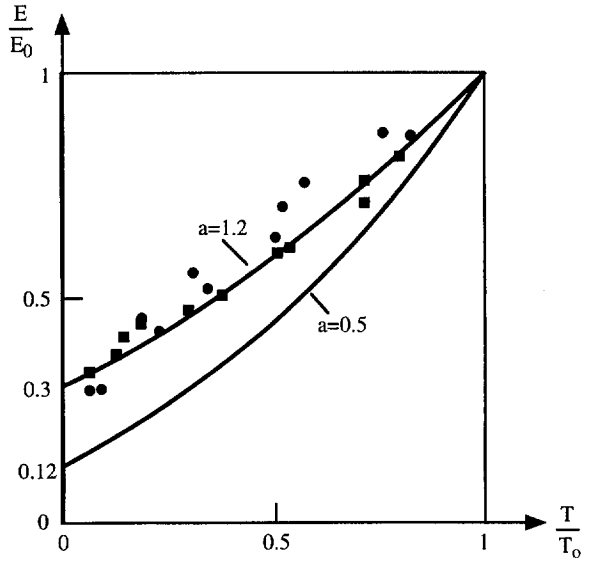

Fig. 16. Relative dynamic stiffness during isotonic shortening at tension T, plotted against relative tension assuming zero slope for the isometric tension–length relation. Stiffness and tension are relative to their isometric values. Solid lines are model predictions (Eq. (38)) with $a = 1.2$ (upper curve) and $a = 0.5$ (lower curve). Points are frog single fibre skeletal muscle at 0°C and 500 Hz (■) or 1 kHz (●) from Julian and Sollins (1975). The relative stiffness at zero tension is 0.3 for $a = 1.2$ or 0.12 for $a = 0.5$.

non-zero stiffness at zero tension (typically 12% of isometric for cardiac muscle at 20°C but about 30% for frog skeletal muscle at 0°C). Using $a = 0.5$, the model predicts $a^2/(1 + a)^2 = 0.11$, in good agreement with experimental observations for cardiac muscle at 20°C. The frog skeletal muscle data at 0°C is fitted by Eq. (38) with $a = 1.2$ as shown in Fig. 16. It is not clear whether the zero tension stiffness (and hence the parameter 'a') is species dependent and/or temperature dependent. The prediction that the relative stiffness versus relative tension relation is independent of the perturbation frequency is also borne out experimentally for both skeletal and cardiac muscle.

3.4. Shortening deactivation

The duration of activation in cardiac muscle is a function of load because the calcium release from troponin C is influenced by crossbridge tension (see Eq. (2)). For example, an isotonic twitch (solid lines) terminates more quickly than an isometric twitch (broken lines), as shown by the model in Fig. 17. In the isotonic phase of the twitch the tension T is lower than the isometric tension T_o and the level of bound Ca quickly drops. As the muscle shortens T_o drops and T/T_o increases, thereby slowing the release of calcium. Shortening stops when T_o equals the applied load T plus the internal compressive load T_p.

Another example of shortening deactivation can be seen when a rapid length step is imposed during an otherwise isometric twitch. Figure 18(a) shows the time course of bound calcium Ca_b during an isometric twitch (solid line) and a 2% length step in 2 ms (broken line). The

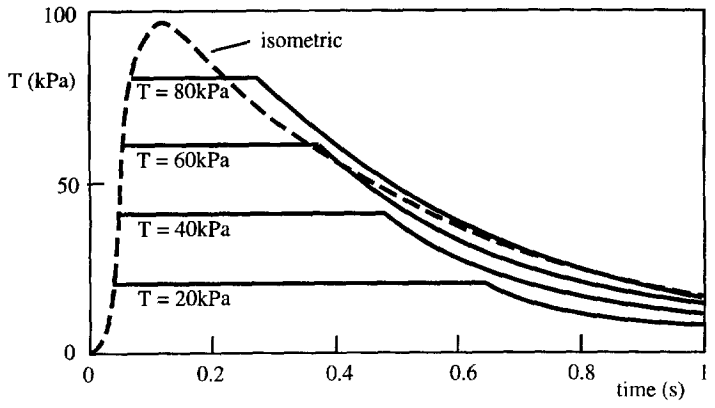

Fig. 17. Isotonic twitch contractions at 20–80 kPa loads (solid lines) compared with an isometric twitch (broken line). Notice the prediction (in agreement with experiment) of a shortened twitch at low loads (the solid line for $T = 20$ kPa lies below the isometric curve) and an enhanced duration of force production at high loads (the solid line for $T = 80$ kPa lies above the isometric curve).

resulting tension responses are shown in Fig. 18(b). Following the length step tension drops to nearly zero, displacing calcium from troponin C so that the post-step isometric tension (broken line in Fig. 18b) is always lower than for the unperturbed isometric twitch (solid line in Fig. 18b).

Not all aspects of shortening deactivation are modelled here because we are prescribing the time course of $[Ca^{2+}]_i$ (Eq. (1)). In a physiological cell the calcium displaced from troponin C by the tension drop would be available for rebinding to TnC but is also rapidly removed from the cytosol by the sarcoplasmic reticular Ca–ATPase pumps. Note that this can also result in a longer action potential because enhanced Na/Ca exchange stimulated by the elevated myoplasmic Ca^{2+} gives an additional inward current during the plateau of the action potential, which is therefore prolonged.

4. Discussion

4.1. Main conclusions

A substantial body of experimental observations on the mechanical performance of cardiac muscle has now been published. In contrast to cardiac electrophysiology, where quantitative models of membrane ion channels and transporters are highly developed, there have been surprisingly few attempts to provide a comparable model for cardiac muscle mechanics. Early empirical models of cardiac muscle mechanics were modified versions of the skeletal muscle models of Hill (1938, 1949) which combined a contractile element obeying a hyperbolic force–velocity relation, a passive series elastic element and a passive parallel elastic element (e.g. Tözeren, 1985; Pinto, 1987). More biophysically motivated models, based on the Huxley (1957) approach of strain dependent rates for crossbridge attachment and detachment, were developed by Wong (1971, 1972), Panerai (1980) and Guccione and McCulloch (1993). All of these

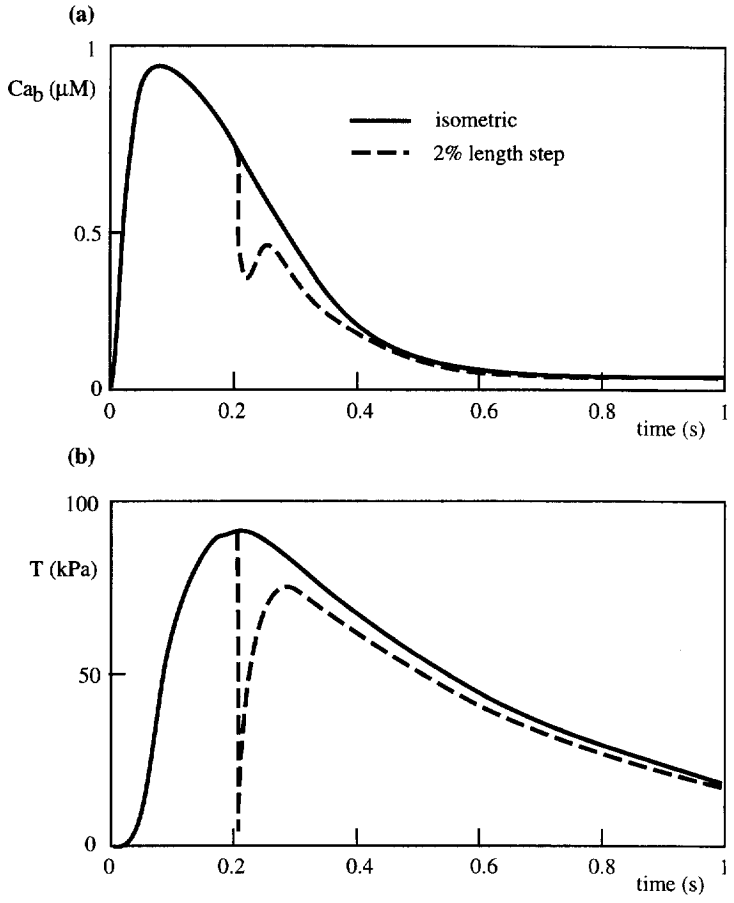

Fig. 18. Effects of shortening deactivation predicted by the model for a quick release experiment. (a) The time course of TnC-bound Ca^{2+} (Ca_b) under isometric conditions (solid line) and following a 2% shortening step (broken line). (b) The corresponding tension responses. See text for details.

models, however, deal only with the rather limited range of experimental tests available at that time. The more recent data, particularly from skinned fibre experiments on which the current model is largely based, are far more comprehensive.

In this paper we have surveyed a wide range of published experimental results on cardiac (and to a lesser extent skeletal) muscle and described a mathematical framework for interpreting these experiments. Many seemingly unrelated results are shown to be different manifestations of the same underlying mechanisms. The mathematical model considers (i) the passive elasticity of cardiac tissue, (ii) Ca-binding to troponin C and its dependence on crossbridge tension, (iii) thin filament kinetics and associated length dependence, and (iv) crossbridge kinetics. The model is based primarily on the measured tension transients following calcium step release experiments and length step experiments but is also shown to correctly predict the response to isotonic loading and sinusoidal stiffness tests.

The experimental observations described by the model are as follows:

- The passive elasticity of cardiac muscle, seen as a tensile load at extension ratios greater than 1 (slack length) and as a compressive load at lengths below slack length (Eqs. (A.3) and (A.4), Fig. 2).
- The dependence of TnC bound calcium on intracellular free calcium and the shift in the binding curve with crossbridge tension (Eq. (3), Fig. 5).
- The transient rise in intracellular free calcium due to detachment of calcium from TnC during quick release experiments (Eq. (2), Fig. 18).
- Isometric tension dependence on length and intracellular calcium concentration (Eqs. (9)–(12), Fig. 8).
- The time course of isometric tension development following step changes in intracellular calcium (Fig. 7) and the dependence of tension redevelopment rate on bound calcium (Eq. (6), Fig. 6).
- The dependence of shortening velocity on load and level of activation (Eq. (29), Fig. 14a).
- The length and activation independence of unloaded shortening velocity at lengths above resting length (Eq. (30), Fig. 14b).
- The reduction of (externally) unloaded shortening velocity at lengths below resting length due to the internal compressive elastic load (Fig. 14b).
- The frequency dependence of dynamic stiffness (magnitude and phase) and the changes in stiffness with changes in level of activation (Eq. (31), Fig. 15).
- The load dependence and frequency independence of high frequency stiffness, measured under isotonic conditions, relative to isometric stiffness (Eq. (38), Fig. 16).
- The shortening deactivation seen with isotonic twitch contractions (Fig. 17) and during rapid length steps (Fig. 18).

4.2. Further development of the model

Here we briefly discuss other aspects of cell physiology which have an influence on cardiac mechanics and which will need to be included in future developments of the model.

4.2.1. Membrane electrophysiology

One clear requirement is to couple the mechanics model presented here to the highly developed models of cardiac cell membrane ion channels and transporters, e.g. the atrial model of Hilgemann and Noble (1987) and the ventricular cell models of Luo and Rudy (1991, 1994). Both electro-mechanical coupling and mechano-electrical coupling must be considered: the calcium induced-calcium release at the T-tubule/SR diadic junctions provides the source of free myoplasmic calcium to replace Eq. (1) (Bers, 1991) and the subsequent mechanical events influence the conductivity of stretch activated channels (see review by Sachs, 1994).

4.2.2. Cardiac energetics

Another future development of the model will be to include a description of chemomechanical transduction. The contractile proteins actin and myosin convert chemical energy from the hydrolysis of ATP into mechanical work. Wannenburg et al. (1997) studied ATP utilisation in skinned rat trabeculae, at various lengths and calcium concentrations, by

measuring the flourescence decay of NADH. (With no mitochondria present the ATP used by the myofilaments was regenerated by oxidation of NADH to NAD.) They found a linear relationship between ATP consumption and isometric tension, with a slope of 15 μM ATP·s^{-1} (kPa)$^{-1}$. Changes in sarcomere length and Ca^{2+} activation had no effect on the slope. Similar results for skeletal muscle have been obtained by Brenner (1988). At a maximum tension of 100 kPa this gives a maximum rate of ATP consumption of 1.5 mM·s^{-1} (ATP is present in cardiac muscle at a concentration of about 7 mM, and is normally buffered by a CrP concentration of 25 mM, see Ch'en et al., 1997, this volume). Since the density of S1 myosin heads in cardiac muscle is about 0.15 mM (He et al., 1997), the ATPase rate is about 10 s^{-1} per myosin head, which correlates well with the speed of maximum unloaded shortening $V_o = 6$ s^{-1} (a measure of maximum crossbridge turnover) discussed in Section 2.3. However, a simple algebraic relationship between tension and ATP consumption may be insufficient: He et al. (1997) report an initial ATPase rate of 6 s^{-1} for rat trabeculae following photorelease of ATP, followed by ATPase rates of 3 and 2 s^{-1} for the second and third turnover of ATP, respectively. Slower, but also time-varying, hydrolysis rates were obtained for skinned guinea pig trabeculae by Barsotti and Ferenczi (1988). Kentish and Stienen (1994) found that force development declined more rapidly than ATPase activity with decreasing sarcomere length in skinned rat myofibrils. They reported a maximum ATPase rate equivalent to an ATP turnover per myosin S1 head of 3.3 s^{-1}. ATP consumption under non-isometric conditions has yet to be determined.

4.2.3. Control of myofilament activation

Myocardial tissues express many different cell surface receptors which ultimately control the inotropic and chronotropic state of the muscle. The influence of these receptors on model parameters must be quantified. There are three major signaling pathways that involve the membrane bound enzymes adenylate cyclase, guanylate cyclase and phospholipase C, respectively, with the corresponding second messengers cAMP, cGMP and DAG (diacylglycerol). In all three cases the second messengers activate protein kinases (PKA, PKG and PKC, respectively) which phosphorylate specific sites on the contractile proteins, membrane channels and pumps (see review by Ishikawa and Homcy, 1997).

β-adrenoreceptor stimulation of adenylate cyclase via G-proteins increases the cAMP-mediated phosphorylation of TnI and TnC by PKA, causing a reduction in the Ca^{2+}-binding properties of TnC (although Blinks, 1993, suggests that the Ca-desensitisation may be achieved by reducing the positive feedback resulting from crossbridge attachment, rather than altering the Ca^{2+} affinity of TnC). β-adrenergic stimulation can be mimicked in skinned fibre preparations by controlling the concentration of PKA. de Tombe and ter Keurs (1991a), de Tombe and Stienen (1995) and Janssen and de Tombe (1997) have shown that PKA has no effect on either isometric tension or the velocity of unloaded shortening (V_o) at sarcomere lengths above slack length (i.e. away from the influence of internal elastic loads). Exposing skinned rat trabeculae to 3 μg/ml of PKA caused a significant increase in the $[Ca^{2+}]_i$ required for half maximal steady state tension development (C_{50}) but both T_o and V_o were unaffected. This indicates that a, A_1 and α_1 are independent of PKA but that C_{50ref} and possibly γ are PKA dependent.

Stimulation of ventricular muscarinic receptors by acetylcholine (or the synthetic agonist carbachol) inhibits adenylate cyclase and therefore has a Ca-sensitising effect. Phosphodiesterase inhibitors, which inhibit cAMP breakdown, provide another means of enhancing Ca-desensitisation. Other consequences of β-adrenoreceptor stimulation are phosphorylation of phospholamdan to accelerate the uptake of intracellular calcium into the SR by Ca-ATPase pumps and an increased rate of release of Ca^{2+} by the ryanodine receptor release sites in the junctional SR. β-agonists are the endogenous catecholamines epinephrine and norepinephrine and the synthetic isoproterenol. The best known β-antagonist is propranolol.

α-adrenoreceptor stimulation of phospholipase C via G-proteins stimulates the production of diacylglycerol (DAG) and inositol trisphosphate (IP_3). Both contribute to the activation of PKC, leading to regulation of many cardiac proteins, including troponin T, the SR Ca^{2+} pump, the Na^+/H^+ exchanger and the L-type Ca^{2+} channel (Solaro, 1993; Pi et al., 1997). Stimulation of guanylate cyclase catalyses the production of cGMP which has been shown to stimulate dephosphorylation of TnI by PKG and therefore increase Ca-sensitivity. By raising $[Ca^{2+}]_i$ IP_3 also activates other Ca^{2+}-dependent enzymes (Lakatta, 1996).

C-protein, associated with the thick filament, is thought to modify the range of movement of crossbridges and thereby have a role in the probability of crossbridge binding, especially at submaximally activating free Ca^{2+}. Cardiac muscle C-protein is phosphorylated in vitro by PKA and in vivo by adrenergic stimulation (Solaro, 1993; Hofmann and Lange, 1994; Gautel et al., 1995).

Cardiac muscle also contains substantial concentrations of 'natural modulators' of contractility, many of which affect the Ca-sensitivity of skinned fibres, e.g. *N*-acetyl anserine, *N*-acetyl carnosine, *N*-acetyl histidine and taurine (Miller et al., 1993).

4.2.4. Myosin isoforms

Accommodating the species dependence of different myosin isoforms and their potential for phosphorylation will require further model development. Cardiac myosin consists of two heavy chains (MHC) and two pairs of light chains (MLC). The LC-2 isoform is mainly expressed in the normal human heart (Morano, 1993; Morano et al., 1995). MLC can be reversibly phosphorylated and is therefore labelled MPLC (MPLC phosphorylation initiates contraction in smooth muscle). The in vivo MPLC phosphorylation level cannot be changed by α- or β-adrenergic stimulation and remains unchanged during diastole and systole in the mammalian heart. Phosphorylation of MPLC increases the force of cardiac contraction but not shortening velocity. Cardiac muscle can express two different myosin heavy chain genes, α and β. The ATPase rate of the $\alpha\alpha$ combination, or V_1 isoform, is twice that of the $\beta\beta$ combination, or V_3 isoform (Pope et al., 1980). Adult rats express the V_1 form whereas adult ferret, guinea-pig and rabbit express the V_3 form. The maximum shortening velocity V_o of human atrial fibres is twice as high as the V_o of human ventricular fibres, suggesting that the rate limiting step which determines V_o is modulated by myosin isoenzymes.

4.2.5. Calcium sensitising cardiac drugs

Most calcium-related drug action on cardiac cells modulates $[Ca^{2+}]_i$ by influencing the release and uptake of calcium, e.g. Bay K-8644 acts as a Ca^{2+} channel agonist by favouring

prolonged opening of the L-type Ca^{2+} channels; caffeine and ryanodine enhance the release of Ca^{2+} from the SR via the ryanodine receptor; the SR Ca^{2+}-ATPase pump is inhibited by thapsigargin and cyclopiazonic acid. However, recent research has focussed on another broad class of inotropic calcium mechanism which is more directly related to mechanics: Ca-sensitivity modulation. Brenner (1993) proposes three classes of Ca-sensitivity modulation: a class I sensitiser increases Ca^{2+}-binding to TnC (e.g. affects the parameter γ in Eq. (2)); a class II(a) sensitiser gives increased Ca^{2+} responsiveness by modulation of thin filament kinetics (e.g. affects α_0 in Eq. (4)); while a class II(b) sensitiser affects crossbridge kinetics (e.g. affects α_1 in Eq. (19)). Examples of class II sensitizers are pimobendan, sulmazole and EMD 53998 (Blinks, 1993). Ca^{2+} sensitivity of the myofilaments can range over about 0.5 pCa units (Solaro, 1993).

Appendix A. The contribution of passive tension during active contraction

For incompressible materials the components of the 2nd Piola–Kirchhoff stress tensor referred to material coordinates and measured per unit area of the undeformed material, are given by

$$T^{MN} = -p\delta^{MN} + \frac{1}{2}\left(\frac{\partial W}{\partial e_{MN}} + \frac{\partial W}{\partial e_{NM}}\right). \tag{A.1}$$

where W is an elastic strain energy function and p is the hydrostatic pressure (Hunter and Smaill, 1989). To accommodate the microstructural observations and biaxial test results we have proposed a strain energy function, called the *pole-zero law* (Hunter et al., 1992), of the form

$$W = k_1 \frac{e_{11}^2}{(a_1 - |e_{11}|)^{b_1}} + k_2 \frac{e_{22}^2}{(a_2 - |e_{22}|)^{b_2}} + k_3 \frac{e_{33}^2}{(a_3 - |e_{33}|)^{b_3}} + k_4 \frac{e_{12}^2}{(a_4 - |e_{12}|)^{b_4}} + k_5 \frac{e_{23}^2}{(a_5 - |e_{23}|)^{b_5}} + k_6 \frac{e_{31}^2}{(a_6 - |e_{31}|)^{b_6}} \tag{A.2}$$

where:

- e_{MN} are the components of the Green strain tensor referred to material coordinates aligned with the structurally defined axes of the tissue (the e_{MN}^2 numerator terms are necessary to ensure non-zero stiffness at zero strain).
- $a_1 \ldots a_6$ are parameters expressing the limiting strain for a particular type of deformation (i.e. the strain energy becomes very large as e_{11} approaches a_1, etc.) and $a_1 > e_{11}$, $a_2 > e_{22}$, $a_3 > e_{33}$, $a_4 > e_{12}$, $a_5 > e_{23}$, $a_6 > e_{31}$.
- $b_1 \ldots b_6$ are parameters expressing the curvature of the uniaxial stress–strain curves (partly a reflection of the distribution of unextended fibre lengths as more collagen fibres are recruited).
- $k_1 \ldots k_6$ are parameters giving the relative contribution of each strain energy term and k_1, k_2, k_3 are defined to be zero if e_{11}, e_{22} or e_{33}, respectively, are negative.

Using a separate pole for each microstructurally defined axis accommodates the different strain limiting behaviour seen along each axis. This strain energy function can be considered as the first part of a polynomial expansion in the pole-zero terms (i.e. terms of the form $W(e) = ke^2/(a-e)^b$). A higher order expansion including cross-product terms may be justified by further experimental testing, particularly of shear behaviour. As it stands there are 18 free parameters in Eq. (A.2) but some of these parameters must be strongly correlated because some tensile and shearing deformations are likely to involve the same underlying collagen microstructure. These parameter correlations are provided by a biophysical model of muscle elasticity in which the strain energy arises from the stretching of several families of collagen fibres, whose distributions are based on observations of tissue microstructure (Hunter et al., 1996b).

The uniaxial tension–length relation is derived here first for tension ($\lambda_1 > 1$) and then for compression ($\lambda_1 < 1$). We consider a cylindrical segment of muscle under the assumption that the material properties in the plane orthogonal to the axis are isotropic (i.e. the muscle is transversely isotropic). Then $\lambda_2 = \lambda_3 = 1/\sqrt{\lambda_1}$ (to maintain the incompressibility constraint $\lambda_1\lambda_2\lambda_3 = 1$) gives

$$e_{11} = \frac{1}{2}(\lambda_1^2 - 1) \quad \text{and} \quad e_{22} = e_{33} = \frac{1}{2}(\lambda_2^2 - 1) = \frac{1}{2}\left(\frac{1}{\lambda_1} - 1\right).$$

For axial tension ($\lambda_1 > 1$) the strain energy function, Eq. (A.2), reduces to

$$W = k_1 \frac{e_{11}^2}{(a_1 - e_{11})^{b_1}}.$$

since e_{22} and e_{33} are negative and therefore W contains no other contribution from fibre stretch.

From Eq. (A.1), $T^{22} = \partial W/\partial e_{22} - p = 0$ gives $p = \partial W/\partial e_{22} = 0$ and the axial 2nd Piola–Kirchhoff stress is

$$T^{11} = \frac{\partial W}{\partial e_{11}} = k_1\left[\frac{2e_{11}}{(a_1 - e_{11})^{b_1}} + \frac{b_1 e_{11}^2}{(a_1 - e_{11})^{b_1+1}}\right],$$

or simplifying,

$$T^{11} = \frac{k_1 e_{11}}{(a_1 - e_{11})^{b_1}}\left[2 + \frac{b_1 e_{11}}{(a_1 - e_{11})}\right]. \tag{A.3}$$

The data in Fig. 2 from Kentish et al. (1986) are fitted with $k_1 = 0.2$ kPa, $a_1 = 0.22$ and $b_1 = 1.0$. Eq. (A.3) with these parameters is shown as the solid line (for $\lambda = \lambda_1 > 1$) in Fig. 2 with the pole at $e_{11} = a_1$ when $\lambda_1 = \sqrt{1 + 2a_1} = 1.2$.

For axial compression ($\lambda_1 < 1$) the strain energy function, Eq. (A.2), reduces to

$$W = 2k_2 \frac{e_{22}^2}{(a_2 - e_{22})^{b_2}},$$

since e_{22} and e_{33} are assumed equal and now e_{11} is negative so there is no contribution from the axial term.

From Eq. (A.1), $T^{22} = \partial W/\partial e_{22} - p = 0$ gives

$$p = \frac{\partial W}{\partial e_{22}} = \frac{2k_2 e_{22}}{(a_2 - e_{22})^{b_2}}\left[2 + \frac{b_2 e_{22}}{(a_2 - e_{22})}\right],$$

and the axial 2nd Piola–Kirchhoff stress is

$$T^{11} = -p = \frac{-2k_2 e_{22}}{(a_2 - e_{22})^{b_2}}\left[2 + \frac{b_2 e_{22}}{(a_2 - e_{22})}\right], \tag{A.4}$$

where $e_{22} = \frac{1}{2}(1/\lambda_1 - 1)$.

This relation (for $\lambda = \lambda_1 < 1$), with parameter values $k_2 = 0.06$ kPa; $a_2 = 0.41$; $b_2 = 2.5$ determined from biaxial loading experiments (Smaill and Hunter, 1991), is shown as a solid line in Fig. 2. Note that the pole at $e_{22} = a_2$ occurs when

$$e_{22} = \frac{1}{2}\left(\frac{1}{\lambda_1} - 1\right) = a_2 \quad \text{or} \quad \lambda_1 = \frac{1}{1 + 2a_2} = 0.55.$$

Appendix B. Dynamic stiffness calculations

B.1. Isometric stiffness

The response of the model to small sinusoidal length perturbations is analysed here. Consider a perturbation of λ of magnitude $\Delta\lambda$ and frequency ω about a mean length of $\lambda = 1$:

$$\lambda = 1 + \Delta\lambda \cdot e^{i\omega t}, \tag{B.1}$$

where ($i = \sqrt{-1}$). To find the corresponding solution to the model equations let

$$z = z^* + \Delta z \cdot e^{i\omega t}, \tag{B.2}$$

$$T = T^* + \Delta T \cdot e^{i\omega t}, \quad (\text{where } T^* = z^* T_{\text{ref}}) \tag{B.3}$$

and

$$Ca_b = Ca_b{}^* + \Delta Ca_b \cdot e^{i\omega t} \tag{B.4}$$

where z^*, T^* and Ca_b^* are the means about which these quantities oscillate with magnitudes Δz, ΔT and ΔCa_b, respectively. The magnitudes are considered as complex numbers in order to accommodate phase shifts relative to the imposed length sinusoid. To find the relationships between Δz, ΔT, ΔCa_b and $\Delta\lambda$, we consider TnC binding kinetics, thin filament kinetics and crossbridge kinetics in turn, since each of these processes has direct or indirect length dependence.

B.1.1. Troponin C binding kinetics

Equation (2) for TnC–Ca^{2+} binding is

$$\frac{dCa_b}{dt} = \rho_0 Ca_i(Ca_{bmax} - Ca_b) - \rho_1\left(1 - \frac{T}{\gamma T_o}\right)Ca_b. \tag{B.5}$$

The effect of a length perturbation on this equation occurs via both the tension T and the isometric tension T_o given by Eq. (9). Substituting Eqs. (B.1) and (B.2) into Eq. (9) gives

$$T_o = T_{ref}(1 + \beta_0(\lambda - 1)) \cdot z = T_{ref}(1 + \beta_0 \Delta\lambda \cdot e^{i\omega t})(z^* + \Delta z \cdot e^{i\omega t})$$

or, omitting terms involving the product of small perturbations,

$$T_o \approx z^* T_{ref} + z^* T_{ref}\left(\beta_0 \Delta\lambda + \frac{\Delta z}{z^*}\right) \cdot e^{i\omega t}. \tag{B.6}$$

Combining Eqs. (B.3) and (B.6), using the binomial theorem $1/1 + \Delta = 1 - \Delta + O(\Delta)^2 \approx 1 - \Delta$ for $\Delta \ll 1$ and omitting the quadratically small product terms,

$$\frac{T}{T_o} \approx 1 + \left(\frac{\Delta T}{T^*} - \frac{\Delta z}{z^*} - \beta_0 \Delta\lambda\right) \cdot e^{i\omega t}. \tag{B.7}$$

Substituting Eqs. (B.4) and (B.7) into Eq. (B.5) gives

$$\frac{Ca_b{}^*}{Ca_{bmax}} = \frac{Ca_i}{Ca_i + \rho_1/\rho_0(1 - 1/\gamma)} \tag{B.8}$$

for the zeroth order (mean) term and

$$i\omega \cdot \Delta Ca_b = -\rho_0 Ca_i \cdot \Delta Ca_b - \rho_1\left(1 - \frac{1}{\gamma}\right) \cdot \Delta Ca_b + \frac{\rho_1}{\gamma} Ca_b{}^*\left(\frac{\Delta T}{T^*} - \frac{\Delta z}{z^*} - \beta_0 \Delta\lambda\right) \tag{B.9}$$

for the perturbation term (neglecting quadratically small terms). Rearranging Eq. (B.9) gives

$$\frac{\Delta Ca_b}{Ca_b{}^*} = \frac{\rho_1/\gamma(\Delta T/T^* - \Delta z/z^* - \beta_0 \Delta\lambda)}{\rho_0 Ca_i + \rho_1(1 - 1/\gamma) + i\omega}, \tag{B.10}$$

which reveals how ΔCa_b depends on the perturbation magnitudes of T, z and λ via a complex impedance which acts as a low-pass filter with a break frequency which varies with Ca_i.

B.1.2. Thin filament kinetics

Equation (4) for thin filament kinetics is

$$\frac{dz}{dt} = \alpha_0\left[\left(\frac{Ca_b}{C_{50}}\right)^n (1 - z) - z\right], \tag{B.11}$$

where the length perturbation dependence of n and C_{50}, from Eqs. (11) and (12) with Eq. (B.1), is

$$n = n_{\text{ref}}(1 + \beta_1 \Delta\lambda \cdot e^{i\omega t}), \qquad pC_{50} = pC_{50\text{ref}}(1 + \beta_2 \Delta\lambda \cdot e^{i\omega t})$$

and therefore

$$C_{50} = 10^{6-pC_{50}} = C_{50\text{ref}} \cdot 10^{-pC_{50\text{ref}}\beta_2 \Delta\lambda \cdot e^{i\omega t}} \approx C_{50\text{ref}} \cdot (1 - \ln 10 \cdot pC_{50\text{ref}}\beta_2 \Delta\lambda e^{i\omega t}).$$

Thus, with Eq. (B.4),

$$\frac{Ca_b}{C_{50}} = \frac{Ca_b^*}{C_{50\text{ref}}}\left[1 + \left(\frac{\Delta Ca_b}{Ca_b^*} + \ln 10 \cdot pC_{50\text{ref}}\beta_2 \Delta\lambda\right) \cdot e^{i\omega t}\right]$$

and raising this expression to the power $n = n_{\text{ref}} + \Delta$ using

$$x^{n_{\text{ref}}+\Delta} \approx x^{n_{\text{ref}}} \cdot (1 + \ln x \cdot \Delta) \quad \text{and} \quad (1+\delta)^{n_{\text{ref}}+\Delta} \approx 1 + \delta \cdot n_{\text{ref}} \quad (\Delta, \delta \ll 1)$$

gives

$$\left(\frac{Ca_b}{C_{50}}\right)^n \approx \left(\frac{Ca_b^*}{C_{50\text{ref}}}\right)^{n_{\text{ref}}}\left[1 + n_{\text{ref}}\left(A\Delta\lambda + \frac{\Delta Ca_b}{Ca_b^*}\right) \cdot e^{i\omega t}\right], \tag{B.12}$$

where

$$A = \beta_1 \ln \frac{Ca_b^*}{C_{50\text{ref}}} + \beta_2 \ln 10 \cdot pC_{50\text{ref}}. \tag{B.13}$$

Substituting Eqs. (B.2) and (B.12) into Eq. (B.11) gives

$$i\omega \Delta z \cdot e^{i\omega t} = \alpha_0\left\{\left(\frac{Ca_b^*}{C_{50\text{ref}}}\right)^{n_{\text{ref}}}\left[1 + n_{\text{ref}}\left(A\Delta\lambda + \frac{\Delta Ca_b}{Ca_b^*}\right) \cdot e^{i\omega t}\right](1 - z^* - \Delta z \cdot e^{i\omega t}) - (z^* + \Delta z \cdot e^{i\omega t})\right\}$$

from which

$$z^* = \frac{(Ca_b^*)^{n_{\text{ref}}}}{(Ca_b^*)^{n_{\text{ref}}} + (C_{50\text{ref}})^{n_{\text{ref}}}} \quad \text{or} \quad \left(\frac{Ca_b^*}{C_{50\text{ref}}}\right)^{n_{\text{ref}}} = \frac{z^*}{1 - z^*} \tag{B.14}$$

and

$$\frac{\Delta z}{z^*} = n_{\text{ref}} \frac{A\Delta\lambda + \Delta Ca_b/Ca_b^*}{1/(z^* - 1) + i\omega/\alpha_0}, \tag{B.15}$$

by equating the zeroth order terms and first order perturbation terms, respectively. Equation (B.15) reveals the low pass filtering characteristics of the equation for thin filament kinetics, Eq. (B.11).

Eliminating ΔCa_b from Eqs. (B.10) and (B.15) gives

$$\frac{\Delta z}{z^*} = \frac{(AB - \beta_0)\Delta\lambda + (\Delta T/T^*)}{1 + BD} \tag{B.16}$$

where

$$B = \gamma \frac{\rho_0}{\rho_1} Ca_i + \gamma - 1 + \frac{\gamma}{\rho_1} i\omega \tag{B.17}$$

and

$$D = \left(\frac{1}{z^* - 1} + i\frac{\omega}{\alpha_0} \right) / n_{ref}. \tag{B.18}$$

B.1.3. Crossbridge kinetics

The equations governing crossbridge kinetics are

$$T = T_0 \cdot \frac{1 + aQ}{1 - Q}, \quad Q = \sum_{k=1}^{3} A_k \int_{-\infty}^{t} e^{-\alpha_k (t-\tau)} \mathring{\lambda}(\tau)\, d\tau. \tag{B.19}$$

Substituting Eq. (B.1) into Eq. (B.19) and neglecting quadratically small terms gives

$$T \approx T_0[1 + (1 + a)Q], \tag{B.20}$$

where

$$Q = \Delta\lambda \cdot \sum_{k=1}^{3} A_k \frac{i\omega}{\alpha_k + i\omega} e^{i\omega t}. \tag{B.21}$$

Substituting Eqs. (B.3), (B.6) and (B.21) into Eq. (B.20) and equating the perturbation terms yields

$$\frac{\Delta T}{T^*} = \left[\beta_0 + (1 + a) \sum_{k=1}^{3} A_k \frac{i\omega}{\alpha_k + i\omega} \right] \cdot \Delta\lambda + \frac{\Delta z}{z^*}. \tag{B.22}$$

B.1.4. Dynamic stiffness

Finally, substituting Eq. (B.16) into Eq. (B.22) and rearranging gives the desired stiffness relation:

$$\mathbf{E} = \frac{\Delta T}{\Delta\lambda} = z^* T_{ref} \left[\beta_0 + \frac{A}{D} + \left(1 + \frac{1}{BD} \right)(1 + a) \sum_{k=1}^{3} A_k \frac{i\omega}{\alpha_k + i\omega} \right], \tag{B.23}$$

where A, B and D are given by Eqs. (B.13), (B.17) and (B.18), respectively.

B.2. High frequency stiffness during isotonic shortening

To determine the predicted dynamic stiffness during a constant velocity (V) shortening, let

$$\lambda = \lambda_o - V \cdot t + \Delta\lambda \cdot e^{i\omega t}, \quad (i = \sqrt{-1})$$

where $\Delta\lambda$ and ω are the amplitude and frequency of the applied length perturbation and we assume that ω is sufficiently high that only crossbridge kinetics need to be considered. As shown above, both TnC–Ca^{2+} binding kinetics and thin filament kinetics act as lowpass filters and do not make significant contributions to stiffness above about 100 s^{-1}. Substituting $\dot{\lambda} = -V + i\omega\Delta\lambda \cdot e^{i\omega t}$ into the right hand side of Eq. (18), extracting the corresponding tension perturbation from the left hand side (using a Taylor series expansion, see Bergel and Hunter, 1979) and putting

$$\Delta\tilde{\lambda} = \Delta\lambda \cdot e^{i\omega t} \quad \text{and} \quad \Delta\tilde{T} = \Delta T \cdot e^{i(\omega t+\phi)}$$

gives $\Delta\tilde{T} = E \cdot \Delta\tilde{\lambda}$, where $E(T, T_o, \omega)$ is the dynamic stiffness:

$$E(T, T_o, \omega) = \frac{T}{T_o} \cdot \frac{dT_o}{d\lambda} + \frac{T_o(T/T_o + a)^2}{1 + a} \cdot \sum_{k=1}^{3} A_k \frac{i\omega}{\alpha_k + i\omega}. \tag{B.24}$$

Note that if $T = T_o$ and $\lambda = 1$, $1/T_o \cdot dT_o/d\lambda = \beta_0$ and Eq. (B.24) reduces to Eq. (B.23) with $1/D -> 0$ at high ω.

If $dT_o/d\lambda = 0$ (corresponding to the plateau of the skeletal muscle isometric tension relation), Eq. (B.24) becomes

$$E(T, T_o, \omega) = \frac{T_o(T/T_o + a)^2}{1 + a} \cdot \sum_{k=1}^{3} A_k \frac{i\omega}{\alpha_k + i\omega}. \tag{B.25}$$

The stiffness of the isometric muscle ($T = T_o$) is then

$$E(T_o, T_o, \omega) = T_o(1 + a) \cdot \sum_{k=1}^{3} A_k \frac{i\omega}{\alpha_k + i\omega}, \tag{B.26}$$

and the relative stiffness, obtained by dividing Eq. (B.25) by Eq. (B.26) is

$$\frac{E(T, T_o, \omega)}{E(T_o, T_o, \omega)} = \left(\frac{T/T_o + a}{1 + a}\right)^2. \tag{B.27}$$

Note that this is independent of frequency, as observed experimentally, and yields the plot, shown in Fig. 16, of relative stiffness versus relative tension in good agreement with experiment on frog single fibre skeletal muscle.

References

Allen, D.G., Kentish, J.C., 1988. Calcium concentration in the myoplasm of skinned ferret ventricular muscle following changes in muscle length. J. Physiol. (London) 407, 489–503.

Allen, D.G., Kurihara, S., 1982. The effects of muscle length on intracellular calcium transients in mammalian cardiac muscle. J. Physiol. (London) 327, 79–94.

Araujo, A., Walker, J.W., 1994. Kinetics of tension development in skinned cardiac myocytes measured by photorelease of Ca^{2+}. Am. J. Physiol. 267 (Heart Circ. Physiol. 36), H1643–H1653.

Araujo, A., Walker, J.W., 1996. Phosphate release and force generation in cardiac myocytes investigated with caged phosphate and caged calcium. Biophys. J. 70, 2316–2326.

Ashley, C.C., Mulligan, I.P., Lea, T.J., 1991. Ca^{2+} and activation mechanisms in skeletal muscle. Q. Rev. Biophys. 24, 1–73.

Backx, P.H., Gao, W.-D., Azan-Backx, M.D., Marban, E., 1995. The relationship between contractile force and intracellular [Ca^{2+}] in intact rat cardiac trabeculae. J. Gen. Physiol. 105, 1–19.

Barany, M., 1967. ATPase activity of myosin correlated with speed of muscle shortening. J. Gen. Physiol. 50, 197–216.

Barsotti, R.J., Ferenczi, M.J., 1988. Kinetics of ATP hydrolysis and tension production in skinned cardiac muscle of the guinea pig. J. Biol. Chem. 263, 16750–16756.

Bergel, D.H., Hunter, P.J., 1979. The mechanics of the heart. In: Hwang, H.H.C., Gross, D.R., Patel, D.J. (Eds.), Quantitative Cardiovascular Studies, Clinical and Research Applications of Engineering Principles. University Park Press, Baltimore, ch. 4, pp. 151–213.

Bers, D.M., 1991. Excitation–contraction Coupling and Cardiac Contractile Force. Kluwer Academic Pubishers, Dordrecht, The Netherlands.

Blinks, J.R., 1993. Analysis of the effects of drugs on myofibrillar Ca^{2+} sensitivity in intact cardiac muscle. In: Lee, J.A., Allen, D.G. (Eds.), Modulation of Cardiac Calcium Sensitivity. OUP, Oxford, pp. 242–282.

Brady, A.J., 1991b. Length dependence of passive stiffness in single cardiac muocytes. Am. J. Physiol. 260, H1062–H1071.

Bremel, R.D., Weber, A., 1972. Cooperation within actin filament in vertebrate skeletal muscle. Nature New Biol. 238, 97–101.

Brenner, B., 1988. Effect of Ca^{2+} on cross-bridge turnover kinetics in skinned single rabbit psoas fibers: implications for regulation of muscle contraction. Proc. Natl. Acad. Sci. USA 85, 3265–3269.

Brenner, B., 1993. Changes in calcium sensitivity at the cross-bridge level. In: Lee, J.A., Allen, D.G. (Eds.), Modulation of Cardiac Calcium Sensitivity. OUP, Oxford, pp. 197–214.

Butters, C.A., Willadsen, K.A., Tobacman, L.S., 1993. Cooperative interactions between adjacent troponin–tropomysin complexes may be transmitted through the actin filament. J. Biol. Chem. 268, 15565–15570.

Ch'en, F.F.-T., Vaughan-Jones, R.D., Clarke, K., Noble, D., 1997. Modelling myocardial ischaemia and reperfusion. Prog. Biophys. Mol. Biol. (this volume).

de Tombe, P.P., Stienen, G.J.M., 1995. Protein kinase A does not alter economy of force maintenance in skinned rat cardiac trabeculae. Circ. Res. 76, 734–741.

de Tombe, P.P., ter Keurs, H.E.D.J., 1990. Force and velocity of sarcomere shortening in trabeculae from rat heart. Effects of temperature. Circ. Res. 66, 1239–1254.

de Tombe, P.P., ter Keurs, H.E.D.J., 1991a. Lack of effect of isoproterenol on unloaded velocity of sarcomere shortening in rat cardiac trabeculae. Circ. Res. 68, 382–391.

de Tombe, P.P., ter Keurs, H.E.D.J., 1991b. Sarcomere dynamics in cat cardiac trabeculae. Circ. Res. 68, 588–596.

de Tombe, P.P., ter Keurs, H.E.D.J., 1992. An internal viscous element limits unloaded velocity of sarcomere shortening in rat myocardium. J. Physiol. 454, 619–642.

DiFrancesco, D., Noble, D., 1985. A model of cardiac electrical activity incorporating ionic pumps and concentration changes. Phil. Trans. R. Soc. London Ser. B: 307, 353–398.

Edman, K.A.P., 1975. Mechanical deactivation induced by active shortening in isolated muscle fibres of the frog. J. Physiol. 246, 255–275.

Endo, M., 1972. Stretch-induced increase in activation of skinned muscle fibres by calcium. Nature New Biol. 237, 211–213.

Fabiato, A., Fabiato, F., 1976. Dependence of calcium release, tension generation and restoring forces on sarcomere length in skinned cardiac cells. Eur. J. Cardiol. 4, 13–27.

Fabiato, A., Fabiato, F., 1978. Myofilament-generated tension oscillations during partial calcium activation and activation dependence of the sarcomere length–tension relation of skinned cardiac cells. J. Gen. Physiol. 72, 667–699.

Ford, L.E., Huxley, A.F., Simmons, R.M., 1977. Tension responses to sudden length change in stimulated frog muscle fibers near slack length. J. Physiol. 269, 441–515.

Fry, C.H., Harding, D.P., Miller, D.J., 1989. Non-mitochondrial calcium ion regulation in rat ventricular myocytes. Proc. R. Soc. London Ser. B: 236, 53–77.

Fuchs, F., 1995. Mechanical modulation of the Ca^{2+} regulatory protein complex in cardiac muscle. NIPS 10, 6–11.

Fuchs, F., Wang, Y.-P., 1996. Sarcomere length versus interfilament spacing as determinants of cardiac myofilament Ca^{2+} sensitivity and Ca^{2+} binding. J. Mol. Cell. Cardiol. 28, 1375–1383.

Fuchs, F., Wang, Y.-P., 1997. Length-dependence of actin–myosin interaction in skinned cardiac muscle fibres in rigor. J. Mol. Cell. Cardiol. 29, 3267–3274.

Gautel, M., Zuffardi, O., Freiburg, A., Labeit, S., 1995. Phosphorylation switches specific for the cardiac isoform of myosin binding protein-C: A modulator of cardiac contraction? EMBO J. 14, 1952–1960.

Gao, W.D., Backx, P.H., Azan-Backx, M.D., Marban, E., 1994. Myofilament Ca^{2+} sensitivity in intact versus skinned rat ventricular muscle. Circ. Res. 74, 408–415.

Granzier, H., Helmes, M., Trombitas, K., 1996. Nonuniform elasticity of titin in cardiac myocytes: A study using immunoelectron microscopy and cellular mechanics. Biophys. J. 70, 430–442.

Granzier, H.L.M., Irving, T.C., 1995. Passive tension in cardiac muscle: Contribution of collagen, titin, microtubules and intermediate filaments. Biophys. J. 68, 1027–1044.

Granzier, H., Kellermayer, M., Helmes, M., Trombitas, K., 1997. Titin elasticity and mechanism of passive force development in rat cardiac myocytes probed by thin-filament extraction. Biophys. J. 73, 2043–2053.

Guccione, J.M., McCulloch, A.D., 1993. Mechanics of active contraction in cardiac muscle: Part I. Constitutive relations for fiber stress that describes deactivation. J. Biomech. Eng. 115, 72–81.

Gulati, J., Sonnenblick, E., Babu, A., 1991. The role of troponin C in the length dependence of Ca-sensitive force of mammalian skeletal and cardiac muscles. J. Physiol. (London) 441, 305–324.

Hancock, W.O., Martyn, D.A., Huntsman, L.L., 1993. Ca^{2+} and segment length dependence of isometric force kinetics in intact ferret cardiac muscle. Circ. Res. 73, 603–611.

Hancock, W.O., Martyn, D.A., Huntsman, L.L., Gordon, A.M., 1996. The influence of Ca^{2+} on force redevelopment kinetics in skinned rat myocardium. Biophys. J. 70, 2819–2829.

He, Z.H., Chillingworth, R.K., Brune, M., Webb, M.R., Ferenczi, M.A., 1997. High time-resolution measurements of ATPase activity during contraction and relaxation in rat cardiac muscle. Biophys. J. 72, A381.

Helmes, M., Trombitas, K., Granzier, H., 1996. Titin develops restoring force in rat cardiac myocytes. Circ. Res. 79, 619–626.

Hess, P., Lansman, J.B., Tsien, R.W., 1984. Different modes of Ca channel gating behaviour favored by dihydropyridine Ca agonist and antagonist. Nature 311, 538–544.

Hibbert, M.G., Jewell, B.R., 1982. Calcium- and length-dependent force production in rat ventricular muscle. J. Physiol. (London) 329, 527–540.

Hilgemann, D.W., Noble, D., 1987. Excitation–contraction coupling and extra-cellular calcium transients in rabbit atrium: reconstruction of basic cellular mechanisms. Proc. R. Soc. London Ser. B: 230, 163–205.

Hill, A.V., 1938. Heat of shortening and the dynamic constants of muscle. Proc. R. Soc. Ser. B: 126, 136–195.

Hill, A.V., 1949. The abrupt transition from rest to activity in muscle. Proc. R. Soc. Ser. B: 136, 399–420.

Hofmann, P.A., Fuchs, F., 1987a. Effect of length and cross-bridge attachment on Ca^{2+} binding to cardiac troponin C. Am. J. Physiol. 253 (Cell Physiol. 22), C90–C96.

Hofmann, P.A., Fuchs, F., 1987b. Evidence for a force-dependent component of calcium binding to cardiac troponin C. Am. J. Physiol. 253 (Cell Physiol. 22), C541–C546.

Hofmann, P.A., Lange, J.H., 1994. Effects of phosphorylation of troponin-I and C protein on isometric tension and velocity of unloaded shortening in skinned single cardiac myocytes from rats. Circ. Res. 74, 718–726.

Holmes, K.C., 1995. The actomyosin interaction and its control by tropomyosin. Biophys. J. 68, S2–S7.

Hunter, P.J., 1995. Myocardial constitutive laws for continuum models of the heart. In: Sideman, S., Beyar, R. (Eds.), Molecular and Subcellular Cardiology. Plenum Press, New York, pp. 303–318.

Hunter, P.J., Nielsen, P.M.F., Le Grice, I.J., Smaill, B.H., Hunter, I.W., 1992. An anatomical heart model with applications to myocardial activation and ventricular mechanics. In: Pilkinton, T.C., Loftis, B., Thompson, J.F., Woo, S.L.-Y., Palmer, T.C., Budinger, T.F. (Eds.), High Performance Computing in Biomedical Research. CRC Press, ch. 1, pp. 3–26.

Hunter, P.J., Smaill, B.H., Nielsen, P.M.F., LeGrice, I.J., 1996a. A mathematical model of cardiac anatomy. In: Panfilov, A., Holden, A. (Eds.), Computational Biology of the Heart. John Wiley Series on Nonlinear Science, ch. 6, pp. 173–217.

Hunter, P.J., Nash, M.P., Sands G.B., 1996b. Computational electro-mechanics of the heart. In: Panfilov, A., Holden, A. (Eds.), Computational Biology of the Heart. John Wiley Series on Nonlinear Science, ch. 12, pp. 347–409.

Hunter, P.J., Smaill, B.H., 1989. The analysis of cardiac function: a continuum approach. Prog. Biophys. Mol. Biol. 52, 101–164.

Huntsman, L.L., Rondinone, J.F., Martyn, D.A., 1983. Force-length relations in cardiac muscle segments. Am. J. Physiol. 244 (Heart Circ. Physiol. 13), H701–H707.

Huxley, A.F., 1957. Muscle structure and theories of contraction. Prog. Biophys. Chem. 7, 255–318.

Huxley, A.F., Simmons, R.M., 1971. Proposed mechanism of force generation in striated muscle. Nature 233, 533–538.

Ishikawa, Y., Homcy, C.J., 1997. The adenyl cyclases as integrators of transmembrane signal transduction. Circ. Res. 80, 297–304.

Janssen, P.M.L., de Tombe, P.P., 1997. Protein kinase A does not alter unloaded velocity of sarcomere shortening in skinned rat cardiac trabeculae. Am. J. Physiol. 273 (Heart Circ. Physiol. 42), H2415–H2422.

Janssen, P.M.L., Hunter, W.C., 1995. Force, not sarcomere length, correlates with prolongation of isosarcometric contraction. Am. J. Physiol. 269 (Heart Circ. Physiol. 38), H676–H685.

Johnson, J.D., Collins, J.H., Robertson, S.P., Potter, J.D., 1980. A fluorescent probe study of Ca^{2+} binding to the Ca^{2+}-specific sites of cardiac troponin and troponin C. J. Biol. Chem. 255, 9635–9640.

Julian, F., Sollins, M.R., 1975. The variation of muscle stiffness with force at increasing speeds of shortening. J. Gen. Physiol. 66, 287–302.

Kentish, J.C., ter Keurs, H.E.D.J., Ricciardi, L., Bucx, J.J.J., Noble, M.I.M., 1986. Comparison between the sarcomere length–force relations of intact and skinned trabeculae from rat right ventricle. Circ. Res. 58, 755–768.

Kentish, J.C., Stienen, G.J.M., 1994. Differential effects of length on maximum force production and myofibrillar ATPase activity in rat skinned cardiac muscle. J. Physiol. 475, 175–184.

Kress, M., Huxley, H.E., Faruqi, A.R., Hendrix, J., 1986. Structural changes during activation of frog muscle studied by time-resolved X-ray diffraction. J. Mol. Biol. 188, 325–342.

Lakatta, E.G., 1996. Regulation of cardiac relaxation. In: Morad, M., Ebashi, S., Trautwein, W., Kurachi, Y. (Eds.), Molecular Physiology and Pharmacology of Cardiac Ion Channels and Transporters. Kluwer, Dordrecht, pp. 481–511.

LeGrice, I.J., Smaill, B.H., Chai, L.Z., Edgar, S.G., Gavin, J.B., Hunter, P.J., 1995. Laminar structure of the heart: ventricular myocyte arrangement and connective tissue architecture in the dog. Am. J. Physiol. 269, H571–H582.

Linke, W.A., Bartoo, M.L., Pollack, G.H., 1993. Spontaneous sarcomere oscillations at intermediate activation levels in single isolated cardiac myofibrils. Circ. Res. 73, 724–734.

Linke, W.A., Popov, V.I., Pollack, G.H., 1994. Passive and active tension in single cardiac myofibrils. Biophys. J. 67, 782–792.

Luo, C.H., Rudy, Y., 1991. A model of the ventricular cardiac action potential: depolarisation, repolarisation, and their interaction. Circ. Res. 68, 1501–1526.

Luo, C.H., Rudy, Y., 1994. A dynamic model of the cardiac ventricular action potential: I. Simulations of ionic currents and concentration changes. Circ. Res. 74, 1071–1096.

MacKenna, D.A., Omens, J.H., McCulloch, A.D., Covell, J.W., 1994. Contribution of collagen matrix to passive left ventricular mechanics in isolated rat hearts. Am. J. Physiol. 266, H1007–H1018.

MacKenna, D.A., Omens, J.H., Covell, J.W., 1996. Left ventricular perimysial collagen fibres uncoil rather than stretch during diastolic filling. Basic Res. Cardiol. 91, 111–122.

Marban, E., Kusuoka, H., Yue, D.T., Weisfeldt, M.L., Weir, W.G., 1986. Maximal Ca^{2+}-activated force elicited by tetanization of ferret papillary muscle and whole heart: Mechanism and characteristics of steady contractile activation in intact myocardium. Circ. Res. 59, 262–269.

Martin, H., Barsotti, R.J., 1994a. Relaxation from rigor of skinned trabeculae of the guinea pig induecd by laser photolysis of caged ATP. Biophys. J. 66, 1115–1128.

Martin, H., Barsotti, R.J., 1994b. Activation of skinned trabeculae of the guinea pig induced by laser photolysis of caged ATP. Biophys. J. 67, 1933–1941.

McCulloch, A.D., 1995. Cardiac biomechanics. In: Branzino, J.D. (Ed.), Biomedical Engineering Handbook. The Electrical Engineering Handbook Series, CRC Press, IEEE Press, Boca Raton, ch. 31, pp. 418–439.

McDonald, K.S., Field, L.J., Parmacek, M.S., Soonpaa, M., Leiden, J.M., Moss, R.L., 1995. Length dependence of Ca^{2+} sensitivity of tension in mouse cardiac myocytes expressing skeletal troponin C. J. Physiol. (London) 485, 131–139.

McDonald, K.S., Moss, R.L., 1995. Osmotic compression of single cardiac myocytes eliminates the reduction in Ca^{2+} sensitivity of tension at short sarcomere lengths. Circ. Res. 77, 199–205.

Metzger, J.M., Moss, R.L., 1990. Calcium-sensitive cross-bridge transitions in mammalian fast and slow skeletal muscle fibres. Science 247, 1088–1090.

Miller, D.J., Lamont, C., O'Dowd, J.J., 1993. Natural calcium-sensitizing compounds of the heart. In: Lee, J.A., Allen, D.G. (Eds.), Modulation of Cardiac Calcium Sensitivity. OUP, Oxford, pp. 115–139.

Morano, I., 1993. Myosin light chain phosphorylation and myosin isoenzyme expression regulate cardiac calcium sensitivity by modulation of cross-bridge cycling rate. In: Lee, J.A., Allen, D.G. (Eds.), Modulation of Cardiac Calcium Sensitivity. OUP, Oxford, pp. 178–196.

Morano, I., Ritter, O., Bonz, A., Timek, T., Vahl, C.F., Michel, G., 1995. Myosin light chain–actin interaction regulates cardiac contractility. Circ. Res. 76, 720–725.

Murphy, E., Steenbergen, C., Levy, L.A., Raju, B., London, R.E., 1989. Cytosolic free magnesium levels in ischaemic rat heart. J. Biol. Chem. 264, 5622–5637.

Pan, B.S., Solaro, R.J., 1987. Calcium-binding properties of troponin C in detergent-skinned heart muscle fibers. J. Biol. Chem. 262, 7839–7849.

Panerai, R.B., 1980. A model of cardiac muscle mechanics and energetics. J. Biomech. 13, 929–940.

Petersen, J.N., Hunter, W.C., Berman, M.R., 1991. Estimated time course of Ca^{2+} bound to troponin C during relaxation in isolated cardiac muscle. Am. J. Physiol. 260 (Heart Circ. Physiol. 29), H1013–H1024.

Pi, Y., Sreekumar, R., Huang, X., Walker, J.W., 1997. Positive inotropy mediated by diacylglycerol in rat ventricular myocytes. Circ. Res. 81, 92–100.

Pinto, J.G., 1987. A constitutive description of contracting papillary and its implications to the dynamics of the intact heart. J. Biomech. Eng. 109, 181–191.

Pope, B., Hoh, J.F.Y., Weeds, A., 1980. The ATPase activities of rat cardiac myosin isoenzymes. FEBS Lett. 118, 205–208.

Robertson, S.P., Johnson, J.D., Potter, J.D., 1981. The time-course of Ca^{2+} exchange with calmodulin, troponin, parvalbumin and myosin in response to transient increases in Ca^{2+}. Biophys. J. 34, 559–569.

Rossmanith, G.H., Hoh, J.F.Y., Kirman, A., Kwan, L.J., 1986. Influence of V_1 and V_3 isomyosins on the mechanical behaviour of rat papillary muscle as studied by pseudo-random binary noise modulated length perturbations. J. Muscle Res. Cell Motility 7, 307–319.

Sachs, F., 1994. Modelling mechanical–electrical transduction in the heart. In: Mow, V.C., Guilak, F., Hochmuth, R.M., Tran-Son-Tay, R. (Eds.), Cell Mechanics and Cellular Engineering. Springer-Verlag, New York, pp. 308–328.

Shiner, J.S., Solaro, R.J., 1984. The Hill coefficient for the Ca^{2+} activation of striated muscle contraction. Biophys. J. 46, 541–543.

Smaill, B.H., Hunter, P.J., 1991. Structure and function of the diastolic heart: Material properties of passive myocardium. In: Glass, L., Hunter, P.J., McCulloch, A.D. (Eds.), Theory of Heart: Biomechanics, Biophysics and Nonlinear dynamics of Cardiac Function. Springer-Verlag, New York, pp. 1–29.

Soeller, C., Cannell, M.B., 1997. Numerical simulation of local calcium movements during L-type calcium channel gating in the cardiac diad. Biophys. J. 73, 97–111.

Solaro, R.J., 1993. Modulation of activation of cardiac myofilaments by beta-adrenergic agonists. In: Lee, J.A., Allen, D.G. (Eds.), Modulation of Cardiac Calcium Sensitivity. OUP, Oxford, pp. 160–177.

Stuyvers, B.D.M.Y., Miura, M., Jin, J.-P., ter Keurs, H.E.D.J., 1997. Ca^{2+}-dependence of diastolic properties of cardiac sarcomeres: involvement of titin. Prog. Biophys. Mol. Biol. (this volume).

ter Keurs, H.E.D.J., Rijnsburger, W.H., van Heuningen, R., Nagelsmit, M.J., 1980b. Tension development and sarcomere length in rat cardiac trabeculae. Evidence of length-dependent activation. Circ. Res. 46, 703–714.

Tözeren, A., 1985. Continuum rheology of muscle contraction and its application to cardiac contractility. Biophys. J. 47, 303–309.

Vandenboom, R., Clarflin, D.R., Julian, F.J., 1997. Plateau in shortening-induced reduction of force redevelopment rate in frog skeletal muscle fibres. Biophys. J. 72, A381.

Vetter, F.J., McCulloch, A.D., 1997. Three-dimensional analysis of regional cardiac function: a model of rabbit ventricular anatomy. Prog. Biophys. Mol. Biol. (this volume).

Walker, J.W., Moss, R.L., 1990. Effects of Ca^{2+} on cross-bridge transitions measured by photogeneration of P_i and ATP (Abstract). Biophys. J. 57, 538A.

Walker, J.W., Lu, Z., Moss, R.L., 1992. Effects of Ca^{2+} on the kinetics of phosphate release in skeletal muscle. J. Biol. Chem. 267, 2459–2466.

Wang, Y.-P., Fuchs, F., 1994. Length, force and Ca^{2+}-troponin C affinity in cardiac and slow skeletal muscle. Am. J. Physiol. 266, C1077–C1082.

Wang, Y.-P., Fuchs, F., 1995. Osmotic compression of skinned cardiac and skeletal muscle bundles: effects on force generation, Ca^{2+} sensitivity, and Ca^{2+} binding. J. Mol. Cell. Cardiol. 27, 1235–1244.

Wannenburg, T., Janssen, P.M.L., Fan, D., de Tombe, P.P., 1997. The Frank-Starling mechanism is not mediated by changes in rate of cross-bridge attachment. Am. J. Physiol. 273 (Heart Circ. Physiol., 42), H2428–H2435.

Wier, W.G., 1990. Cytoplasmic calcium in the mammalian ventricle: dynamic control by cellular processes. Ann. Rev. Physiol. 52, 467–485.

Winegrad, S., 1980. The importance of passive elements in the contraction of the heart. In: Baan, J., Arntzenius, A.C., Yellin, E.L. (Eds.), Cardiac Dynamics. Martinus Nijhoff, The Hague, pp. 11–12.

Wolff, M.R., McDonald, K.S., Moss, R.L., 1995. Rate of tension development in cardiac muscle varies with level of activator calcium. Circ. Res. 76, 154–160.

Wong, A.Y.K., 1971. Mechanics of cardiac muscle, based on Huxley's model: mathematical simulation of isometric contraction. J. Biomech. 4, 529–540.

Wong, A.Y.K., 1972. Mechanics of cardiac muscle, based on Huxley's model: mathematical simulation of active state and force–velocity relation. J. Biomech. 5, 107–117.

Yue, D.T., Marban, E., Weir, W.G., 1986. Relationship between force and intracellular $[Ca^{2+}]$ in tetanized mammalian heart muscle. J. Gen. Physiol. 87, 223–243.

Zeng, J., Laurita, K.R., Rosenbaum, D.S., Rudy, Y., 1995. Two components of the delayed rectifier K^+ current in ventricular myocytes of the guinea pig type: Theoretical formulation and their role in repolarization. Circ. Res. 77 (1), 140–152.

Zot, H.G., Guth, K., Potter, J.D., 1986. Fast skeletal muscle skinned fibers and myofibrils reconstituted with N-terminal fluorescent analogues of troponin-C. J. Biol. Chem. 261, 15883–15890.

Zot, H.G., Potter, J.D., 1987. Calcium binding and fluorescence measurements of dansylaziridine-labelled troponin C in reconstituted thin filaments. J. Muscle Res. Cell Motility 8, 428–436.